Piston Ring Friction Analysis from Oil Film Thickness Measurements

by

Eric J. Deutsch

Bachelor of Science in Mechanical Engineering
Carnegie Mellon University
(1991)

Submitted to the Department of Mechanical Engineering in Partial Fulfillment of the Requirements for the Degree of

MASTER OF SCIENCE IN MECHANICAL ENGINEERING

at the

Massachusetts Institute of Technology

February, 1994

Signature of Author _____
Department of Mechanical Engineering
7 January, 1994

Certified by _____
Wai K. Cheng
Associate Professor, Department of Mechanical Engineering
Thesis Supervisor

Accepted by _____
Ain A. Sonin
Chairman, Departmental Graduate Committee

(This page has been intentionally left blank.)

Piston Ring Friction Analysis from Oil Film Thickness Measurements

by Eric J. Deutsch

Submitted to the Department of Mechanical Engineering on 14 January, 1994 in partial fulfillment of the requirements for the Degree of Master of Science in Mechanical Engineering

ABSTRACT

The oil film behavior of a series of fifteen lubricating oils was tested in a single cylinder spark ignition engine. The oil film thickness between the piston and cylinder liner of this engine was observed using the Laser Induced Fluorescence (LIF) technique. The data was examined for correlations between physical properties of the oil and characteristics of the oil film.

The region of the oil film trace near the top piston ring was analyzed in detail. The film thickness under the top ring decreases with increasing oil viscosity and increasing surface tension. The trend with viscosity is contrary to the classical lubrication theory. These behaviors are explained in terms of the effects of viscosity and surface tension on the transport of oil to the upper cylinder liner. It is this transport process that determines the film thickness under the top ring. Therefore, the supply of oil regulated by the oil control ring and the wiping action of the entire ring pack become important parameters in the top ring friction and wear question.

A theoretical model of top ring lubrication was applied to this data. The model uses classical lubrication theory to solve the ring wetting problem with a novel boundary condition involving the surface tension of the lubricant. With ring, engine, and lubricant data as input, the model calculates the way the oil wets the ring and the resulting friction. Thus, friction was estimated for the tested lubricants. Because of lack of visible wetting profiles in the data and lack of experimentally measured friction, confirmation of the model using the data was not possible. Finally, the computer model was employed in a parametric study to find the theoretical trends between film thickness/friction and viscosity/surface tension.

Thesis Supervisor: Wai K. Cheng
Title: Associate Professor of Mechanical Engineering

(This page has been intentionally left blank.)

ACKNOWLEDGMENTS

My work at the Sloan Automotive Lab was made gratifying by the presence of interesting people who guided me through the rigors of M.I.T. life. Dr. Wai Cheng, with his humor and insight, helped mold the thesis. Dr. David Hoult's technical suggestions were helpful during the experimental phase of work.

Throughout the past couple of years, my fellow graduate students have filled my soul with a warmth that combats the chill of Boston winter. Byron Shaw showed me the ropes in the lab, helped me through my first few courses, and best of all cooked good bar-be-que. Beth Shaw was a lot of fun even while she tolerated the antics of Byron and me. Jim Ryan and I shared the humor that lifted us through rough days at the lab. Clem Sayers commiserated with me about M.I.T. on numerous occasions and helped me survive my first semester of graduate school. Christophe Hochede, the French scientist, was ready for anything wild and crazy--a good trait to have when hanging around me. Jon Fox always had helpful words to say during times of crisis or times of partying. Janice Dearlove put up with my insanity and often helped me collect my thoughts to do research work. Finally I appreciate my roommates, Alan Shihadeh and Serge Brussovansky, who have been the best of friends to me.

The rest of the lab students, including Leon, Kuo-Chiang, Ed, Kyoungdoug, Kristine, Doug, Haissam, Pete, Mark, Mike N., Mike S., Goro, and Tian have all been supportive and friendly. Special thanks go to Joan Kenney who puts up with relentless requests for help, to Brian Corkum, the "Redbone" man, who knows everything about setting up an engine experiment, and to Mr. Viktor Dubrowski who machines parts with precision and care.

This work has been supported by the M.I.T. Research Consortium on Lubrication in Internal Combustion Engines; members are Dana Corporation, Ford Motor Company, Pennzoil Products Company, Peugeot, Renault, and Shell Oil Company. Dr. Clare Huang, Dr. Tayeb Benchaita, Dr. Frances Lockwood, and Dr. Selda Gunsel, all at Pennzoil, have been extremely generous in sharing their expertise during this research.

Eric Deutsch
7 January, 1994

(This page has been intentionally left blank.)

TABLE OF CONTENTS

LIST OF FIGURES

LIST OF TABLES

NOMENCLATURE

	Definition [Units]
a	Radius of ring face [m]
b	Wetted width [m]
B	Full ring width [m]
h_0	Minimum oil film thickness under ring [m]
h_1	Inlet wetting height [m]
h_2	Outlet wetting height [m]
h_∞	Far upstream oil film thickness [m]
L	Ring elastic tension per unit length [N/m]
P_1	Crown land pressure [Pa]
P_2	Second land pressure [Pa]
Ta	Taylor number [non-dimensional]
U	Piston velocity [m/s]
x	Distance along ring [m]
x_1	Inlet wetting location [m]
x_2	Outlet wetting location [m]
x_1^*	Non-dimensional inlet wetting location
x_2^*	Non-dimensional outlet wetting location
Γ_1	Non-dimensional inlet wetting height
Γ_2	Non-dimensional outlet wetting height
μ	Dynamic viscosity [kg/m-s]
σ	Dynamic surface tension [N/m]
σ, σ_0	Low strain rate surface tension [N/m]
$\bar{\sigma}$	Non-dimensional exit dynamic surface tension gradient
τ_{es}	Exit free surface shear stress [N/m^2]

CHAPTER 1: Introduction

1.1 Motivation

The oil film that supports the piston ring against the cylinder liner in a reciprocating internal combustion engine is of essential importance to the friction and wear characteristics of the ring and liner. The entire ring pack, comprising top, second, and oil control rings, accounts for between one-third and one-half of total engine mechanical rubbing friction [1]. It is thus desirable to understand the nature of this oil film in the interest of friction reduction.

1.2 Background

On the theoretical side, Azzola [2] developed a computer code to calculate the solution to the Reynolds formulation of the sub-ring lubricant flow problem. This code incorporates a novel boundary condition at the film detachment point. The exit boundary condition assumes a finite shear stress exists on the lubricant free surface behind the ring. This shear stress is balanced by a dynamic surface tension gradient. The surface tension increases from its nominal low strain rate value a few millimeters downstream of the ring to a much higher value as the high strain rate exit region is approached. The code takes as input (see nomenclature list for explanation of symbols) μ, σ, U, P_1, P_2, L, a, B, and either h_0 or h_∞ and returns ring wetting dimensions x_1, x_2, and either h_0 or h_∞, whichever was not input.

Experimental data on liner oil film behavior has been taken by numerous researchers at M.I.T. and the University of Wisconsin. They have used the Laser-Induced Fluorescence (LIF) technique wherein the oil is doped with a laser-sensitive fluorescent dye, a laser is fired at the point of interest, and the return fluorescence is

measured. The magnitude of the return signal is directly proportional to film thickness for films less than about 100 microns. The theory behind the LIF method is detailed in [3]. At M.I.T. over the years 1990 through 1992, Bliven, Ingles, and Shaw refined the LIF apparatus, converting it from conventional to fiber optics and increasing its signal-to-noise ratio. In its present incarnation, vertical resolution is on the order of one-tenth of a micron and horizontal resolution is on the order of fifty microns.

1.3 New Contribution

Up to now, all experiments employed a single cylinder diesel engine manufactured by Kubota and an uncontrolled set of test oils from various lubricant manufacturers. The current work uses a single cylinder spark-ignition engine made by Kohler and a matrix of experimental lubricants with well controlled viscosity and surface tension. In this gasoline engine, better liner temperature control is possible than in the past.

The thrust of this work is to survey experimentally designed lubricants that vary in surface tension and viscosity for their ring/liner oil film behavior with the goal of examining trends between ring wetting dimensions and oil properties. Another facet of the experiment is to ascertain whether similar oil film phenomena appear in a spark-ignition engine as appear in a compression-ignition engine. If the wetting phenomena are the same, then Azzola's computer analysis, which is based on diesel engine data, can be applied to predict ring friction for the spark-ignition engine data from the new batch of oils. Along the way, improvements are made to Azzola's code enabling it to run more efficiently and accurately.

CHAPTER 2: Experiment

2.1 Kohler Engine Setup

Figure 2-1 is a schematic of the Kohler engine with associated instrumentation. The Kohler model CH14 single-cylinder, spark-ignition engine is rated at 10.5 kW power output. Other relevant characteristics are given in Table 2-1. This all-aluminum motor is relatively advanced in design. It has push-rod actuated overhead valves and piston dimensions representative of a modern automobile engine.

Type:	Single cylinder, horizontal crankshaft, originally air cooled, spark ignition, with overhead valves
Cooling System:	Water cooling to liner, air cooling to head
Lubrication System:	Wet sump, gerotor pump, paper filter, oil/water heat exchanger
Ignition System:	Flywheel magneto
Power:	10.5 kW (14 hp) @ 3600 rpm
Peak Torque:	28.9 N-m (21.3 lbf-ft)
Bore:	87 mm (3.43 in)
Stroke:	67 mm (2.64 in)
Connecting Rod Length	113 mm (4.45 in)
Displacement:	398 cm^3 (24.3 in^3)
Compression Ratio:	8.5:1
Typical Application:	Lawn tractor

Table 2-1 Kohler engine description.

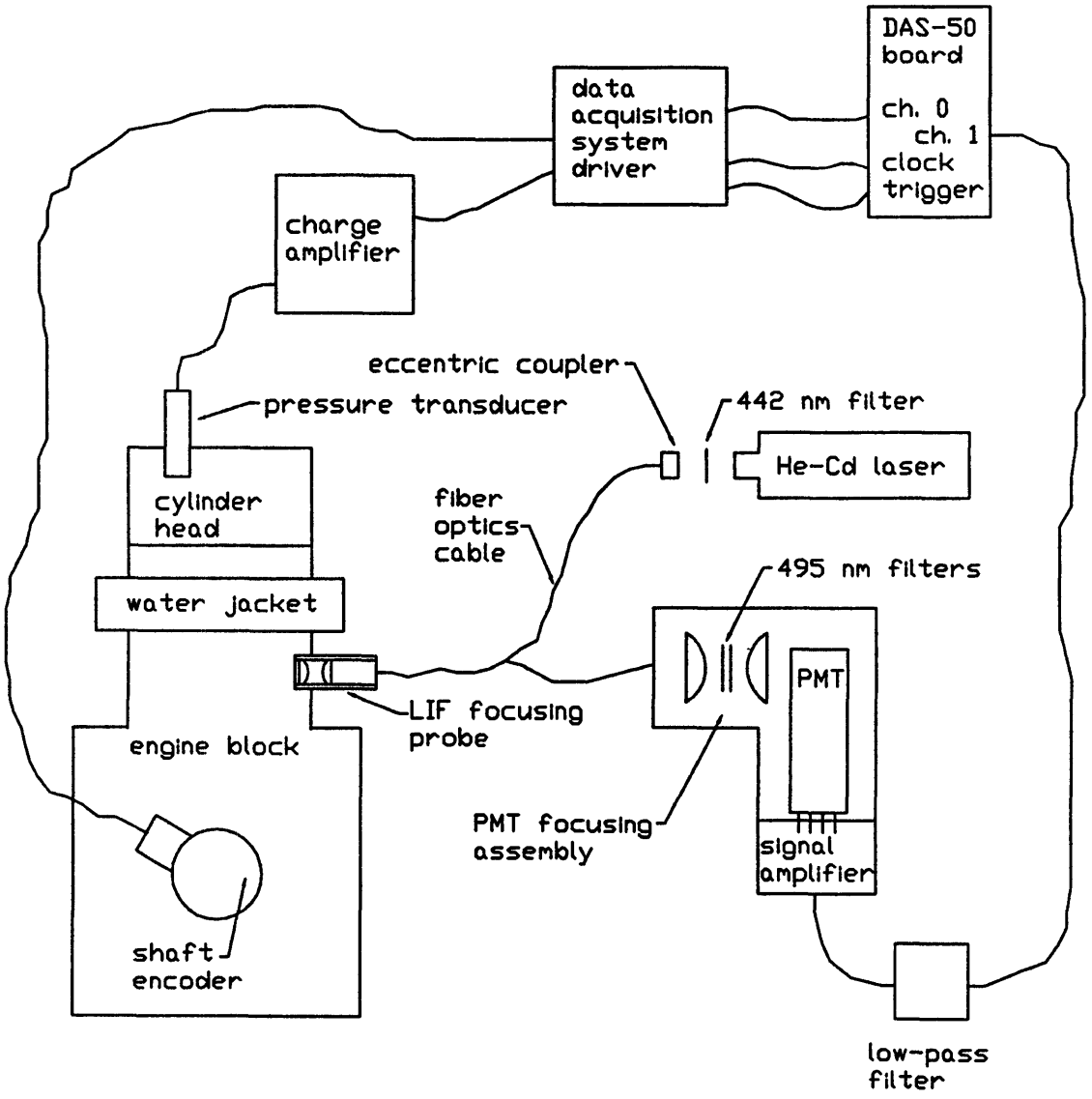

Figure 2-1 Kohler engine set-up and instrumentation.

The ring configuration for the Kohler piston is typical of a light-duty internal combustion engine. There are three rings. The top compression ring (1.5 mm wide) is barrel-faced with parallel sides. The second ring (also 1.5 mm wide) has a tapered face, positive twist, and parallel sides. The oil control ring is a three-piece design with two thin rails (each 0.5 mm wide) and an expander.

A water jacket was added to the originally air-cooled cylinder exterior for liner temperature control. An oil cooler was inserted into the oil flow circuit in order to get an estimate of heat rejected to the oil. Thermocouples were placed at inlets and outlets of the water jacket and oil cooler in order to determine heat rates. Additional thermocouples in the sump and cylinder liner aided in temperature control. The thermocouple locations are: 1) liner coolant in, 2) liner coolant out, 3) oil coolant in, 4) oil coolant out, 5) hot oil out, 6) cooled oil in, 7) engine sump, and 8) cylinder liner.

The instrumentation comprises the LIF probe port mounted in the block on the thrust side of the liner, the pressure transducer mounted in the cylinder head, and the shaft encoder connected to the crankshaft. The shaft encoder is a BEI Motion Systems model H25 that puts out a TTL channel with 2000 pulses per revolution and a TTL channel with a once per revolution top center (TC) pulse. The TC pulse is synchronized with the engine by rotating the encoder relative to the engine until the TC pulse coincides with the peak of the motored pressure signal on an oscilloscope. The piezoelectric pressure transducer is manufactured by Kistler (model 6051A) and was calibrated on a hydraulic rig. The charge output of the transducer is converted to signal voltage by a charge amplifier. Additional instrumentation which is actually part of the dynamometer controller includes a load cell for measuring engine load torque and a hall-effect sensor on the output shaft of the engine for measuring speed.

2.2 The LIF System

The LIF system is driven by a Liconix model 4214NB He-Cd continuous wave laser at 442 nm wavelength. Refer to Figure 2-1 for components of the LIF apparatus. The laser beam passes through a 442 nm narrow band-pass filter before being focused and aligned into the end of a single 50 micron optical fiber by an eccentric coupler. The 442 nm light is carried to the engine by the fiber where it exits the fiber and passes through a focusing probe which collimates the divergent laser light from the fiber and focuses it to a 50 micron spot at the oil film between the piston and cylinder liner.

The LIF focusing probe is detailed in Figure 2-2. The probe screws into a stainless steel threaded sleeve mounted in the engine block. These parts were designed anew for application to the Kohler engine. This probe is smaller than the previous generation probe in order to fit the tight space requirements of the Kohler engine. Its dimensions are optimized for laser light path, fluorescence collection, and engine mounting adaptability. The lenses keep the laser light, with its 28 degree included angle of divergence from the optical fiber, within the small diametrical confines of the probe barrel and focus the return fluorescence within the 28 degree acceptance angle of the collection fibers. The sleeve is installed after drilling and tapping the engine block around the liner. A flat is machined onto the outer surface of the iron liner, and the stainless steel sleeve screws up against this flat. The probe screws into the sleeve with a locknut to hold it in position, allowing for focusing by changing the distance between the probe and the liner.

A small stepped quartz window affords optical access to the cylinder oil film. The liner position and dimensions of this window are given in Figures 2-3 and 2-4. Installation of this window into the engine block requires precise machining of the stepped hole and careful mounting of the window. The mounted window must be flush with the inner surface of the liner, and its curvature must match that of the liner. As a

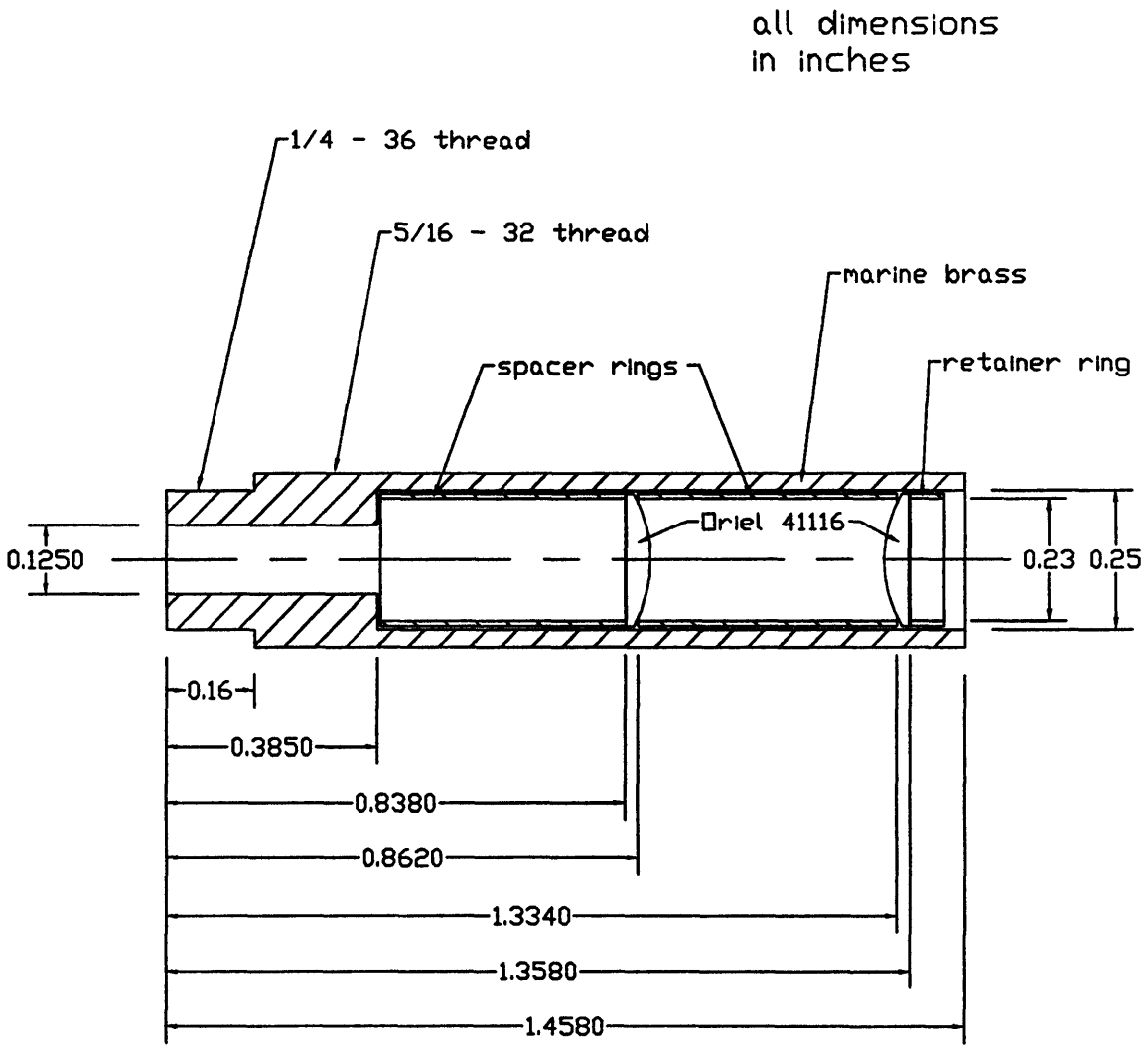

Figure 2-2 LIF focusing probe assembly.

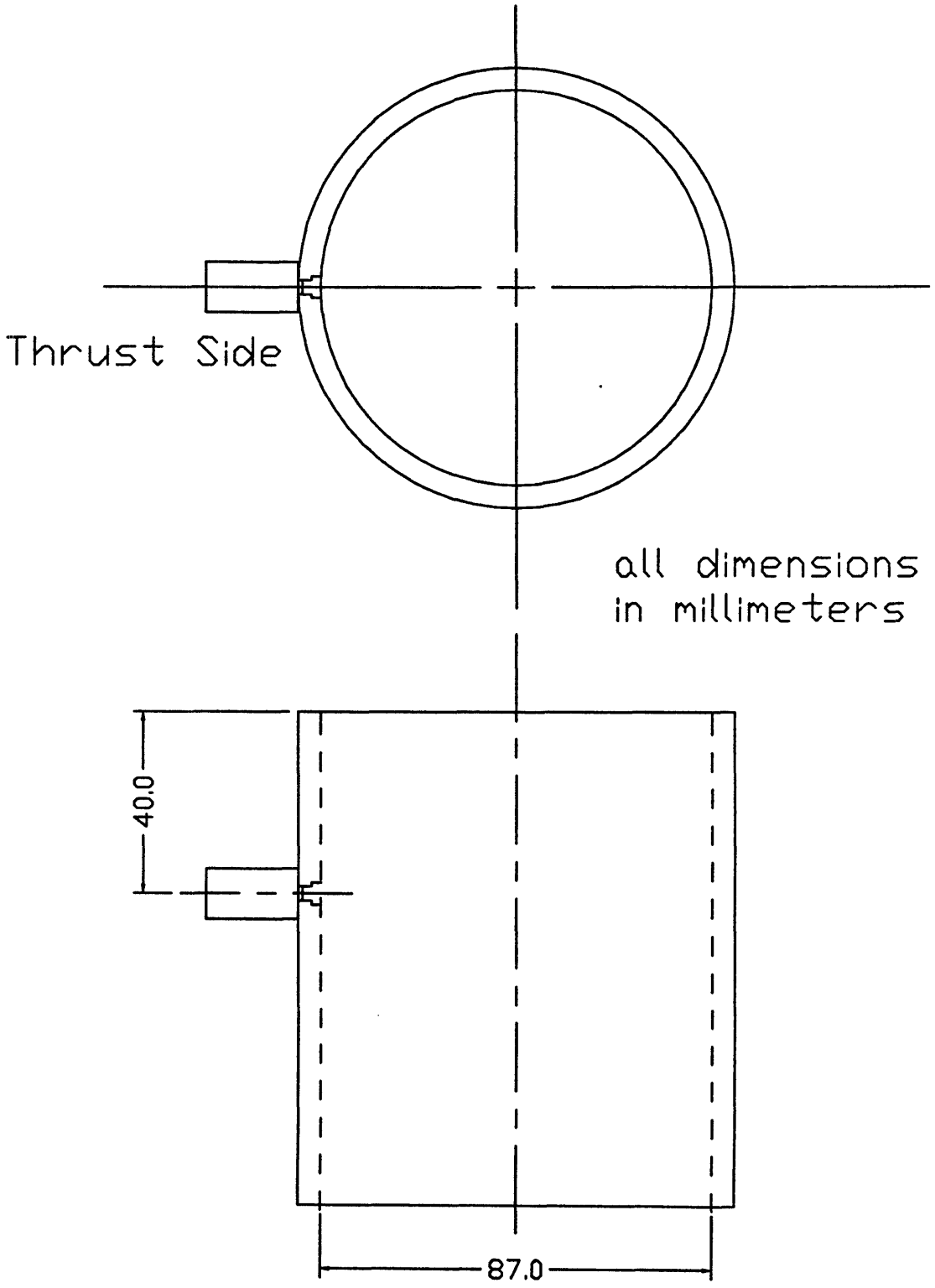

Figure 2-3 LIF probe location in Kohler liner.

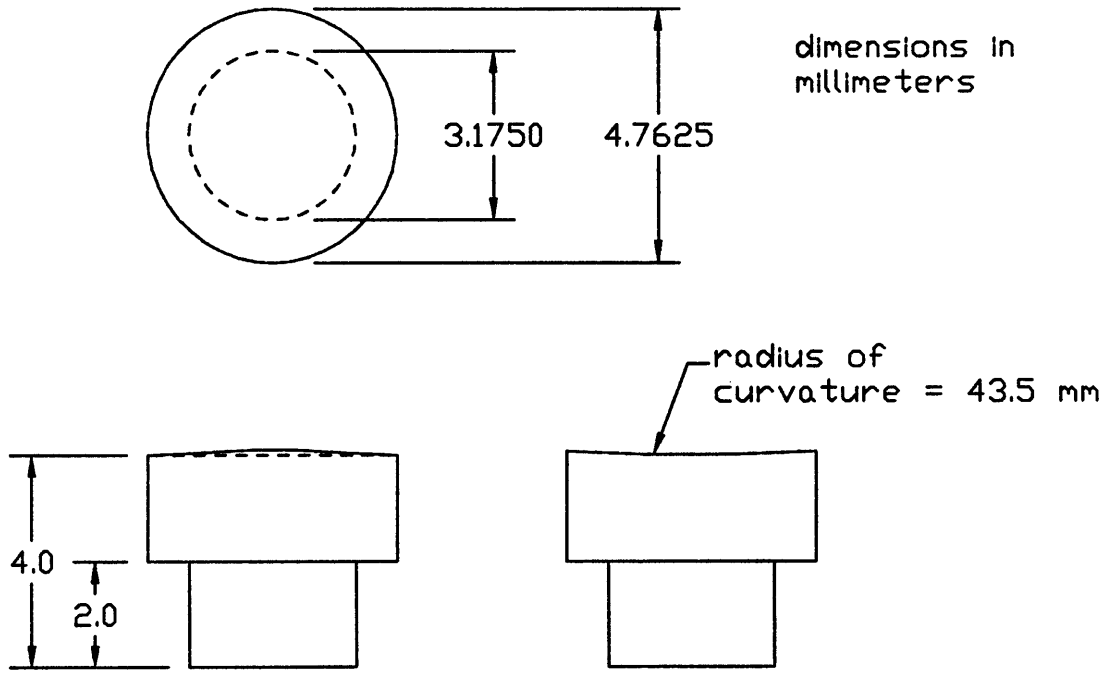

Figure 2-4 Quartz window dimensions.

final step, the cylinder is honed with the window in place in order to minimize liner surface discontinuity.

The oil that is hit by the laser spot has been doped with a fluorescent dye whose wavelength of maximum absorptivity is 442 nm and whose wavelength of maximum fluorescence is 495 nm. When excited by laser light at 442 nm wavelength, the dye gives off light at 495 nm wavelength. This return fluorescence passes back through the probe to eighteen 100 micron collection fibers that surround the 50 micron laser fiber. These fibers travel as a bundle for the co-axial portion of the fiber optics cable until the collection fibers break away from the laser fiber and terminate at the photomultiplier tube (PMT) focusing assembly.

The divergent 495 nm fluorescent signal emerging from the ends of the collection fibers is collimated by a lens, filtered by two narrow band-pass filters, and focused by another lens onto the light-sensitive area of the PMT. A commercial PMT amplifier converts the weak current output of the tube (on the order of nanoamps) into signal voltage in the range of zero to ten Volts. Also, a low-pass filter is employed in the LIF signal line to eliminate some high frequency (>100000 Hz) PMT noise. Complete coverage of the development of the fiber optics LIF apparatus used in this experiment is given by Shaw, Hoult, and Wong [4].

LIF signal intensity depends on many factors including incident laser beam power, alignment of the laser beam into the 50 micron fiber, fluorescent dye concentration, clarity of the oil, temperature of the oil, length of time the oil is exposed to the laser beam, attenuation of the light due to optical filters, and PMT high voltage. These variables are optimized according to the lessons learned from the development of the system over the past few years. For this experiment, dye concentration was 0.00015 mole/L, and oil temperature was in the range of 50 to 100 degrees C. The photobleaching effect is a decay of the LIF signal over time when an oil sample is

suddenly exposed to the laser beam. Researchers at M.I.T. [3] and Shell Research [9] have found time constants for signal decay ranging from 2 to 30 seconds. The severity of decay scales with laser power. In this experiment, oil replenishment occurs in milliseconds and laser power is low. These two factors combine to render the bleaching effect negligible.

2.3 The Data Acquisition System

A PC-based acquisition system was used to collect data in this experiment. A Keithley Metrabyte DAS-50 board was installed in an IBM clone with a 486 processor. The DAS-50 takes up to four channels with 12 bit resolution. Over a range of 0 to 10 Volts, 12 bit resolution means that the smallest discernible voltage difference is 2.44 mV. At typical LIF calibration coefficients, this translates into better than 0.1 micron vertical resolution--more than adequate to reveal detailed features of the oil film. The maximum throughput of the board is 1 MHz; split over two channels, each channel can be sampled at a maximum rate of 500 kHz. The two channels taken are 1) a combined exhaust stroke TC index and cylinder pressure signal and 2) the LIF signal.

The data acquisition system is clocked by the aforementioned BEI optical shaft encoder at a rate of 2000 pulses per revolution. 2000 data points per revolution yields about 10 points per millimeter across the top ring. A horizontal resolution of 0.1 mm is sufficient to provide a good picture of the oil film. With a maximum engine speed of 3600 rpm, the highest required sampling rate per channel is 120 kHz--well below the 500 kHz capacity available.

Although the encoder provides 2000 pulses per revolution, the DAS-50 clocks the two channels sequentially so that connecting the encoder output directly to the board results in only 1000 data points per revolution for each channel. Also, the two channels are not sampled simultaneously: the data points are staggered in time.

Furthermore, the shaft encoder has no way of distinguishing between TC pulses for the exhaust and compression strokes, which would result in data sets being triggered randomly from two different points in the engine cycle. For these reasons, a data acquisition system driver card was built to trigger and clock the DAS-50 board properly.

The driver card is rack mounted separate from the PC. The card takes input from the shaft encoder and pressure charge amplifier. It generates multiple clock pulses for each of the shaft encoder's 2000-per-revolution pulses. For two channels, the board puts out two clock pulses for each shaft encoder pulse. For four channels, the board puts out four clock pulses for each shaft encoder pulse. The output pulses are two microseconds apart, which is half of the DAS-50's 1 MHz capability but fast enough to mimic simultaneous sampling. This burst of pulses allows data to be taken from multiple channels at each of 2000 separate points within one engine revolution.

Since the TC pulse comes once every revolution while the engine cycle is two revolutions long, triggering the data sets from the TC pulse would result in some sets starting from TC of the gas exchange revolution and others starting from TC of the power revolution. It is preferable to start all data sets from the same point in the engine cycle. The driver card accomplishes this by examining the pressure signal. The feature that distinguishes the gas exchange revolution from the power revolution is the cylinder pressure. At each TC pulse, the driver card checks whether the pressure signal is above a preset threshold. If so, then the card knows it is looking at a power revolution and it masks the TC pulse. Therefore, the data sets always begin from TC of the gas exchange stroke. The card also combines the pressure and TC shaft index signals into a composite signal, which saves one channel of data collection.

Table 2-2 gives a description of all the equipment used in the experiment.

Engine	Kohler CH14, 0.4 liter
Dynamometer	Dynamatic IU
Dynamometer Controller	Digalog 1022A STD
LIF:	
He-Cd Laser	Liconix 4214NB
Laser Power Supply	Liconix 4200PS
Laser Filter	Omega Optical 442DF10
Laser Power Meter	Liconix 45PM
Eccentric Coupler	General Fiber Optics 85-22
Fiber Optics Cable	General Fiber Optics 2B16-50/100-2.5-SMA
Focusing Probe, Sleeve, and Locknut	custom made with Oriel 41116 lenses
Quartz Window	Gould Precision Optics special order
Fluorescence Filter	Omega Optical 495DF20
PMT Focusing Lens Mount	Oriel 7132
PMT	Hamamatsu R446
PMT High Voltage Power Supply	Sorenson 1006-10
PMT Signal Amplifier	Hamamatsu C1053
PMT Signal Amplifier 15V Power Supply	custom built
PMT Signal Low-Pass Filter	custom built
Fluorescent Dye	Exciton Coumarin 523
Data Acquisition System:	
PC Board	Keithley Metrabyte DAS-50
Signal Interface	Keithley Metrabyte BNC-50

Shaft Encoder	BEI Motion Systems H25E-F18-SS-2000-ADZC-8830-LED-SM18-S
Driver Card	custom built
Pressure Measurement:	
Pressure Transducer	Kistler 6051A
Charge Amplifier	Kistler 503D
Temperature Measurement:	
Thermocouples (8)	Omega K-type
Thermocouple Readout	Omega 175

Table 2-2 Complete equipment specification.

2.4 Experimental Procedure

A number of lubricants were tested in this experiment. For each lubricant, the following procedure was executed. The oil fill volume for the Kohler engine was determined to be 2 liters. The dye is mixed to achieve the concentration specified by Lux in his thesis [5]. The dye does not dissolve directly into the oil, so an intermediate mixing agent, dichloromethane (CH_2Cl_2), is used. 0.15 grams of Coumarin 523 dye (manufactured by Exciton, Inc.) in powder form is dissolved into 75 milliliters of dichloromethane. This mixture is poured into 2 liters of test oil and shaken vigorously for about a minute.

The dyed oil is poured into the engine which has been flushed of the previous test oil according to a specific procedure. The engine is then motored at 1200 rpm until oil pressure rises to its normal level of about 40 psi. With fuel shut off and the throttle

wide open, the speed is dialed up to 1800 rpm. The engine runs at this speed for about thirty minutes allowing temperatures to stabilize.

Before the first data set is taken. the LIF system must be tuned. The laser having been warmed up for an hour, its output power is checked. A power level of around 12 milliwatts is satisfactory. The fiber-in laser power is checked against the fiber-out laser power to determine how well the laser beam is aligned into the entry of the 50 micron laser fiber. If transmission is below 80 percent, the eccentric coupler is adjusted to maximize fiber-out power.

The engine end of the fiber optics cable is plugged into the focusing probe. The output signal of the LIF apparatus is examined on an oscilloscope with the engine motoring. To focus the laser spot, the LIF signal is maximized by turning the focusing probe in its sleeve thereby adjusting the distance between the probe and the inner surface of the quartz window. Once proper focus is found, the probe is locked into place with a locknut. The high voltage on the PMT is adjusted so that peaks of the LIF signal fall in the 8 to 9 Volt range (the data acquisition board only reads up to 10 Volts).

With the laser adjusted and pressure charge amplifier warmed up, the instrumentation is ready to take a set of data. After data is acquired and all temperatures and flowrates recorded, the engine speed and load are reset to the next running condition: 2500 rpm motored. After the temperature stabilization period, the second motored data is acquired.

The fuel is turned on; the dynamometer is set to absorb load; and the engine fires at 1800 rpm, 5 N-m load torque. Water is supplied to the liner jacket and oil cooler. Once temperatures level off at their new values, the liner coolant flowrate is adjusted to achieve a liner temperature of 100 degrees C, and the next data set is taken. The method for the remaining fired data sets is the same.

When all the data sets for a particular oil, say OIL-A, have been acquired, the engine must be flushed in order to prepare it to receive the next oil, say OIL-B. The flushing procedure begins with a complete drain of hot OIL-A. The engine is refilled with a low viscosity industrial standard flushing oil. The engine is fired at low load to get the sump temperature up to about 60 degrees C and to wash the crankcase with splashing action. The first flushing oil is drained and a second flushing oil run is made.

After the second flush is drained, the oil filter is removed. A compressed air blow adapter was designed and built to screw onto the oil filter base. The air blow device clears out oil passages throughout the engine. After the air blow, a new oil filter is installed, and the crankcase is filled with OIL-B. The engine is again fired until warm, and the first quantity of OIL-B is drained. Finally, the batch of dyed OIL-B test oil for the next data set is added.

The flushing procedure can be summarized as follows:

1. Drain previous oil.
2. Fill with flushing oil, run until warm, drain.
3. Repeat step 2.
4. Change filter, blow with compressed air.
5. Fill with new test oil, run warm, drain.
6. Fill with dyed test oil for data run.

2.5 Lubricant Matrix

The lubricant test matrix spans fifteen oils. Six of the oils, labeled OIL-A through F, vary in viscosity and surface tension. The other nine oils labeled OIL-1 through 9 are based upon OIL-A, which is comparable to SAE grade 5W-30; they vary only in surface tension. The purpose of OIL-A through F is to assess the effect of gross

viscosity changes on oil film behavior. OIL-1 through 9 are meant to isolate the effect of surface tension on oil film behavior.

2.6 Running Condition Test Matrix

For each of the oils, a data set was taken for six engine running conditions covering two speeds and three loads. These running conditions are listed in Table 2-3.

Speed (rpm)	Running Condition
1800	motored
1800	fired at 5 N-m load
1800	fired at 10 N-m load
2500	motored
2500	fired at 10 N-m load
2500	fired at 20 N-m load

Table 2-3 Running conditions.

At 1800 rpm the maximum load the engine would support was about 12 N-m, so half-load (5 N-m) and a full-load (10 N-m) load torques were chosen. At 2500 rpm the maximum load was about 23 N-m, hence the 10 N-m and 20 N-m loads. The liner temperature was maintained at 100 degrees C for all fired cases.

Since there are 6 running conditions and 15 oils, 90 data sets were recorded. Each data set consists of 20 consecutive engine cycles. There are 2000 sampling points in each revolution, 2 revolutions in each cycle, so each data set contains 80000 separate numbers for pressure signal and 80000 separate numbers for LIF signal.

CHAPTER 3: Data Reduction

3.1 LIF Data Analysis Spreadsheet

Raw data sets recorded by the DAS-50 acquisition board contain two columns (one for the combined pressure/TC shaft index signal and one for the LIF signal) of numbers on a scale from 0 to 4096 (2^{12}). These data sets are read into a Microsoft Excel spreadsheet template for conversion into meaningful dimensions. This spreadsheet accepts one engine cycle of data (four strokes), plots the oil film traces for all four strokes, and facilitates calibration of the LIF signal. The LIF spreadsheet is the tool used to display and analyze film behavior.

Every 2000 rows in a data file correspond to one engine revolution (the shaft encoder dictates 2000 sample points per engine revolution); therefore the crank angle between successive rows is 360/2000 = 0.18 degrees. Every data set begins with a trigger pulse at TC of the intake stroke, so the crank angle of all sample points relative to the intake stroke TC index is known. The spreadsheet uses the standard geometric formula for piston position as a function of crank angle to calculate the distance from the top of the piston crown to the laser spot. This enables plotting the LIF signal as a function of distance along the piston and a typical plot is shown in Figure 3-1.

The y-axis of the oil film trace has been converted from raw data to film thickness. Since zero offset scales with tube voltage, the spreadsheet reads in a cycle of zero offset data corresponding to the tube voltage at which the data set was taken. The zero offset is subtracted from the LIF signal, then the signal is converted to voltage. A cell in the spreadsheet allows the user to input a calibration coefficient which gets applied to the entire film trace in order to convert it from voltage to thickness. Raw

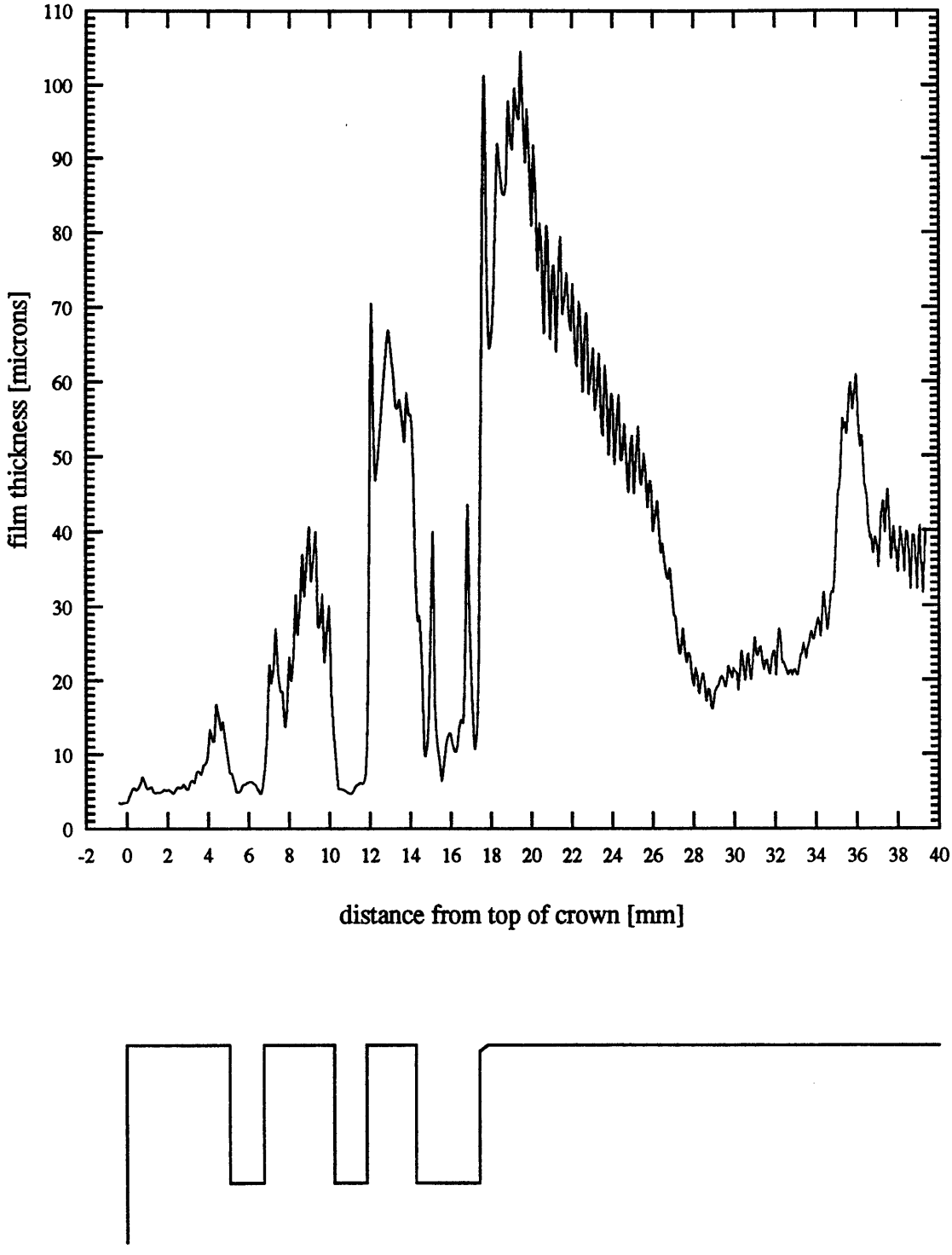

Figure 3-1 Typical LIF trace, 0 - 40 mm on piston. OIL-A, 1800 rpm, motored, compression stroke, averaged data. Below, piston outline showing location of ring grooves.

pressure data is converted to Pascal units in similar fashion. The voltage to pressure conversion factor was determined using a bench calibration rig prior to the experiment.

Calibration and ring fitting require that the microgeometry of the piston skirt tool marks and ring faces be overlaid on the oil film traces. The surface contours of the piston and rings are measured using a Talysurf profilometer. The profiles are digitized and entered into Excel spreadsheets with provisions that their x and y positions can be adjusted. The main LIF spreadsheet calls on these piston skirt and ring profiles so that they are superimposed on the oil film trace. The combination of position adjustment of the profiles and variable vertical scaling of the oil film trace by the calibration coefficient allows the film trace to be matched up against the profiles for calibration or ring fitting.

Excel macros were written to ease reading data sets and zero offset data into the spreadsheet. Data sets are twenty engine cycles long, but the LIF data analysis spreadsheet only holds one cycle. Therefore, the data must be examined one cycle at a time. The macros pick out individual cycles from a twenty cycle data set and insert them into the spreadsheet. In the case of an averaged data set, the twenty cycles have been combined into one cycle, so the entire averaged set fits in the spreadsheet.

The macro which reads the zero offset data also performs another function. Zero offset data introduces extra noise into the top ring film traces, so the macro takes an average of the zero offset in the top ring region and applies that single value to the region. The effect is a smoother film trace, which is important for a detailed ring fit.

3.2 Interpreting a Film Trace

Most piston features are identifiable by their characteristic imprint on the oil film trace. Moving from the top of the piston down in Figure 3-1, the first noteworthy contour is the small lump of oil ahead of the top ring. The area of the top ring (between

5 and 6.7 mm) is characterized by a local minimum in the film thickness trace. Careful inspection of the dip in the film reveals a slight peak at 6 mm in the middle of the sub-ring trace. This behavior of the film defies fitting a radiused top ring face into the trace because the curvature of the film trace is opposite to that of the ring. This leads to problems in reading wetting dimensions.

The jagged contour below the top ring is the oil accumulation on the second land of the piston, and the jagged teeth correspond to machining marks on the second land. These tool marks are also present on the skirt of the piston. The skirt machining marks turn out to be a useful calibration feature.

The dip in the film between 10 and 12 mm marks the passage of the second ring. The tapered face of the second ring does not readily fit itself into this local film minimum. The second ring fit is even less plausible than the top ring fit. The failure to get a second ring fit forced the focus on the top ring for data analysis. Farther down on the piston lies a 60 micron thick lump of oil followed by the distinctive thin rails of the oil control (OC) ring. The two sharp depressions in the film between 14 and 18 mm very closely match the Talysurf profile of the OC ring. In fact, these rails appear so consistently in the data that they are used as an x-axis reference point.

In most cases the OC rails and the other two rings fall where they should according to the locations of the ring grooves as measured directly from the actual piston. In some cases, especially on traces from intake strokes, the film trace features appear about 0.5 mm higher up on the piston than they should. This upward shift could be due to the piston being flung upward to the upper limit of crank pin and wrist pin bearing slop when there is no above-atmospheric cylinder pressure to resist the piston's inertia, and/or it could be due to angular rotation of the piston about the wrist pin axis. Whatever the case, the shift causes error in the distance along the piston calculated from shaft encoder crank angle. In these shifted cases, it is especially important to have the

OC rails as a reference point in the oil film trace. Once the position of the OC rails has been determined, the positions of the other two rings are known from the locations of their grooves on the piston relative to the OC ring groove.

Below the OC ring is the thick oil film of the piston skirt region. Once again the tool marks present themselves as a jagged ripple in the film trace. The taper in film thickness between 20 and 28 mm could be due to a combination of the barrel shape of the skirt, the motion of the piston within the bore, and deformation of the skirt against the liner.

Two final notes: it is important to understand that although the film trace looks like an instantaneous snapshot of the oil film along the piston, it is actually a sequence of points through time. The laser sits at a fixed position in the cylinder liner, and the piston goes by the window. Each point on the film trace represents the amount of oil between the piston and a point 40 mm from the top of the liner. A second word of caution when viewing a film trace is that the LIF system reads only the volume of oil being irradiated by the laser beam and has no response to gas. Since there can be bubbles or gaseous voids between the piston and window, the film thickness trace does not necessarily represent the distance between the piston and the cylinder liner or even the shape of a lubricant film free surface. The problems associated with gaseous voids and bubbles are covered by McElwee in his thesis [7].

3.3 Determination of Calibration Method

Various methods for in-situ calibration of the LIF system have been implemented by researchers in the past. The idea is to match a part of the oil film trace against the known microgeometry of the piston and scale the film trace so that it duplicates the piston feature. These techniques differ in which feature of the piston is examined. The possibilities include second land machining marks, second ring contour

[4, 6, 7], etch marks added to the skirt [6], lower skirt machining marks, and upper skirt machining marks [5, 8].

In the current data sets, only one of these options gives good results. The second land machining marks would be an attractive option because their temperature is close to that of the top ring; however, they are not consistently flooded with oil in this engine. The second ring contour, which was used successfully for calibration in several previous experiments, proves indiscernible in the present film traces. Although the Kohler piston skirt was chemically etched prior to data collection, the 10 and 20 micron deep etch marks do not reliably appear in the film traces, perhaps due to the edges of the marks not being sharp enough or due to a peculiarity of the lubricant flow in this particular engine. The lower skirt machining marks are well flooded with oil but get worn down during the course of the experiment. The only remaining option is the upper skirt tool marks, which always show up well and are not subject to wear.

The upper skirt tool marks are in a region of ample oil supply below the OC ring and are somewhat recessed from the outermost diameter of the skirt due to the skirt's characteristic barrel shape. The use of the upper skirt tool marks for calibration is similar to the method employed by Lux [5].

Once this calibration feature was selected, the data sets were calibrated by importing single cycles into the data analysis spreadsheet. Individual rather than averaged cycles are used because of the potential for obtaining a specious calibration coefficient from an averaged film trace. An averaged trace contains some traces in which oil is fully flooding the region and some in which oil is not flooding the region. When flat non-flooded traces are averaged in with flooded traces, the result is to bring down the peak-to-peak height of the contour. A calibration coefficient determined from a flattened average trace is erroneous.

Calibration is an iterative scheme in which a coefficient is guessed, the oil film trace compared to the micro-profile of the skirt tool marks, and the coefficient revised until the film trace features best match the piston's actual surface features. The result is an overlay such as in Figure 3-2. Notice that the match is not perfect, but reasonably good agreement between the contours is achieved. In particular, the peak-to-peak height is matched well, even though resolution problems with the oil film trace prevent seeing all of the peaks and valleys. It is the vertical height match that is crucial to getting good calibration coefficient.

In all, about 100 data sets were calibrated encompassing all of the fired running conditions and a few of the motored ones. The focus was on the fired cases because these are the cases for which the liner temperature was fixed at 100 degrees C. The oil properties are precisely known at this temperature. Also, fired cylinder conditions are of more interest because they reflect the situation in a running engine.

3.4 Definition of Wetting Dimensions

Before moving on to the results of data reduction, it is important to define the parameters of interest. Several variables are required to completely describe the way oil wets the top ring. Figure 3-3 illustrates the coordinate system and relevant wetting dimensions. The oil film height variables are h_{∞}, the film height far upstream of the ring; h_0, the minimum film thickness under the ring; h_1, the inlet film height; and h_2, the outlet film height. The horizontal dimensions are x_1, the inlet location; x_2, the outlet location; b, the wetted width; and B, the full ring width.

3.5 Failure of Ring Profiles to Appear in Film Traces

The original intent of ring pack data reduction was to obtain detailed wetting information for the top and second rings. It was hoped that all wetting dimensions such

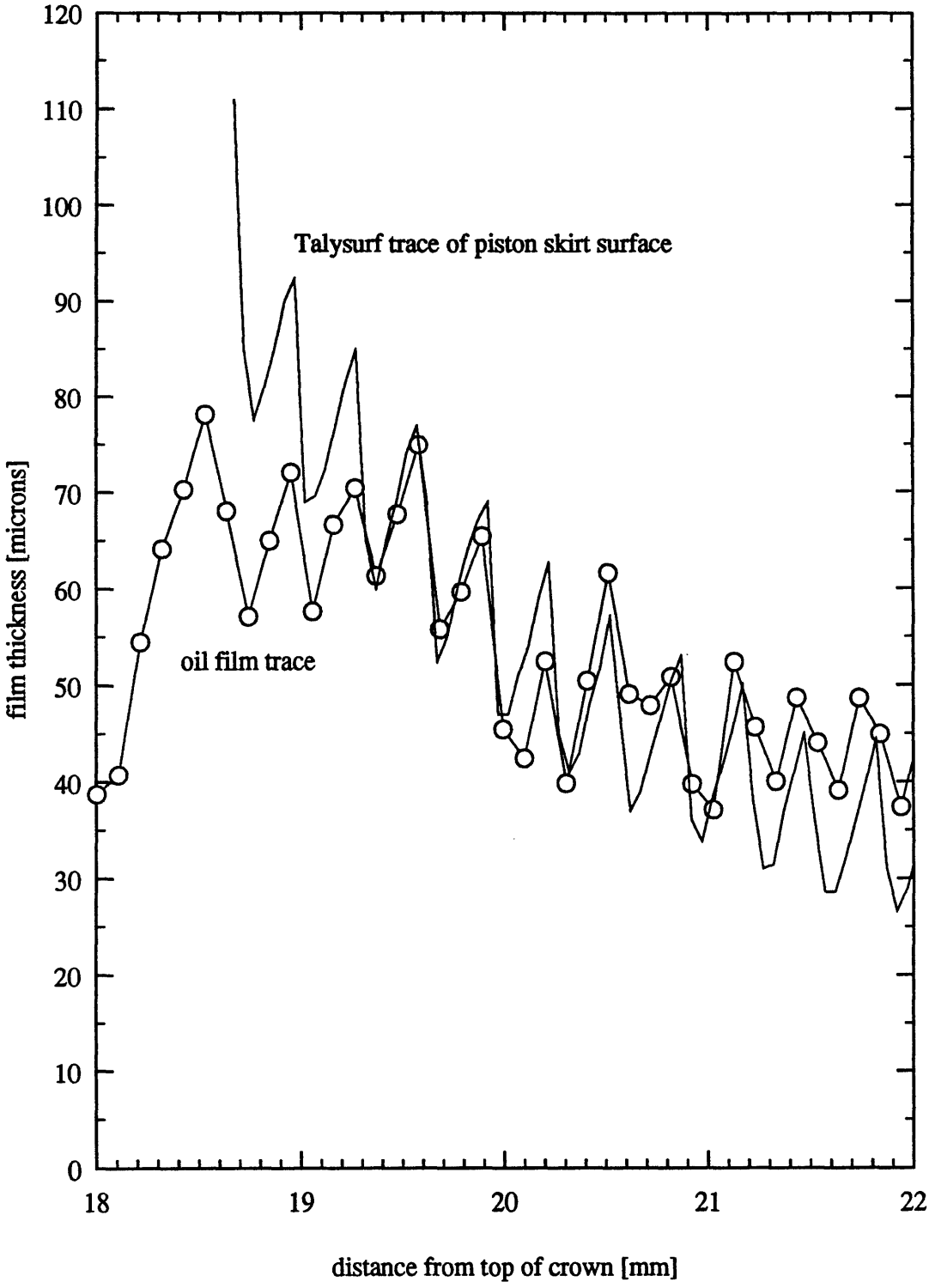

Figure 3-2 Top of skirt machining marks overlaid on oil film trace for calibration (single trace). Circle plotting symbols represent LIF data sampling points.

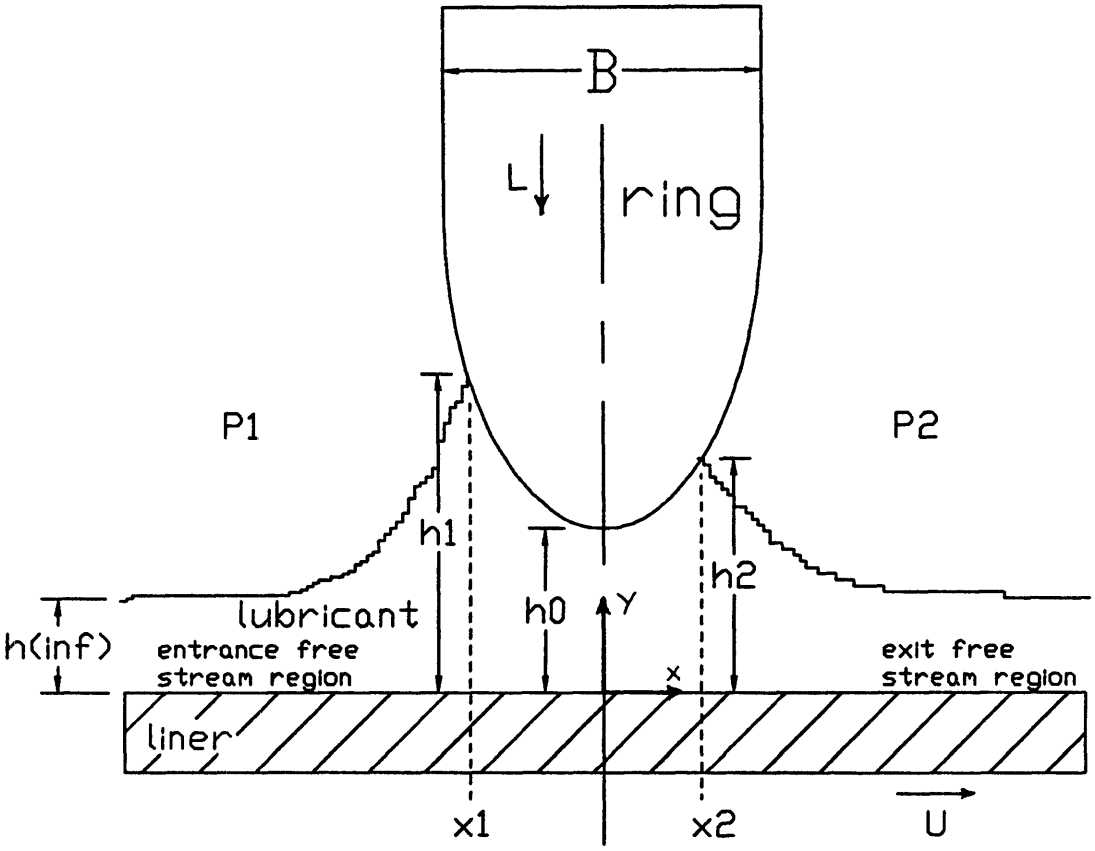

Figure 3-3 Wetting variables and other important parameters.

as h_∞, h_0, h_1, h_2, x_1, x_2, and b could be read from the data. With all these dimensions, the Azzola ring wetting solver (to be discussed later) could have been checked for agreement with the experiment, and estimates of ring friction could have been made with confidence. Unfortunately, due either to the poor quality of the data or to ring loading problems, good ring fits are difficult to find in the data. Random noise on the order of 1 micron makes it hard to distinguish a ring outline in the single film traces. When a trace is averaged over 20 cycles, much of the noise disappears; however, the film traces still fail to display depressions into which the ring profiles might fit.

The data base was searched for top ring fits, but the results were meager. After examining hundreds of single traces from all running conditions and oils, only a few good fits were found. Figure 3-4 shows one of the better fits, one in which the wetted width calculated from the top ring oil flow model is fairly close to the experimentally measured value. However, Figure 3-4 is an atypical case. Traces where the exit film height is higher than the inlet height are sometimes found in the data but are theoretically impossible since this would mean that the ring load is not supported by hydrodynamic lift force; the ring is being sucked into the liner. More typically, the tip of the radiused ring face appears to rest on a peak in the oil film as illustrated in Figure 3-5. This configuration also fails to support the ring elastic and pressure load.

The situation is better with the top ring than with the second ring, so the focus turns to analysis of the top ring data. For lack of a better course of analysis, it was decided that the data should be scrutinized for whatever dimensions it might yield. The only dimensions that can be read from the data with any level of confidence are h_∞ and h_0. Either one of these two variables can be fed to the Azzola code along with other lubricant, engine, and ring parameters in order to solve for theoretical values of all the other wetting dimensions. Given a theoretical prediction of all wetting dimensions,

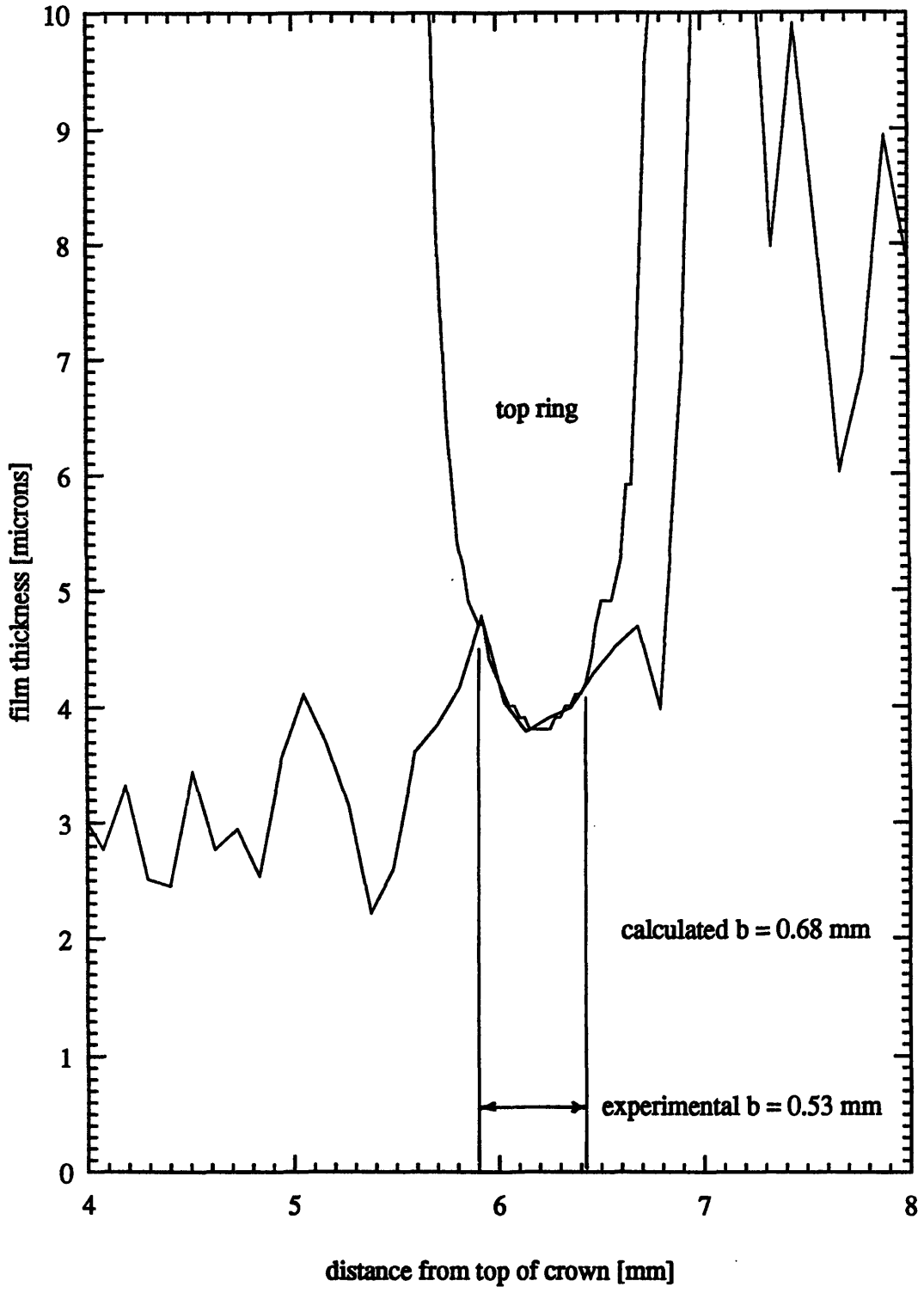

Figure 3-4 Example of good ring fit. OIL-8, 2500 rpm, 20 N-m load, compression stroke, single trace.

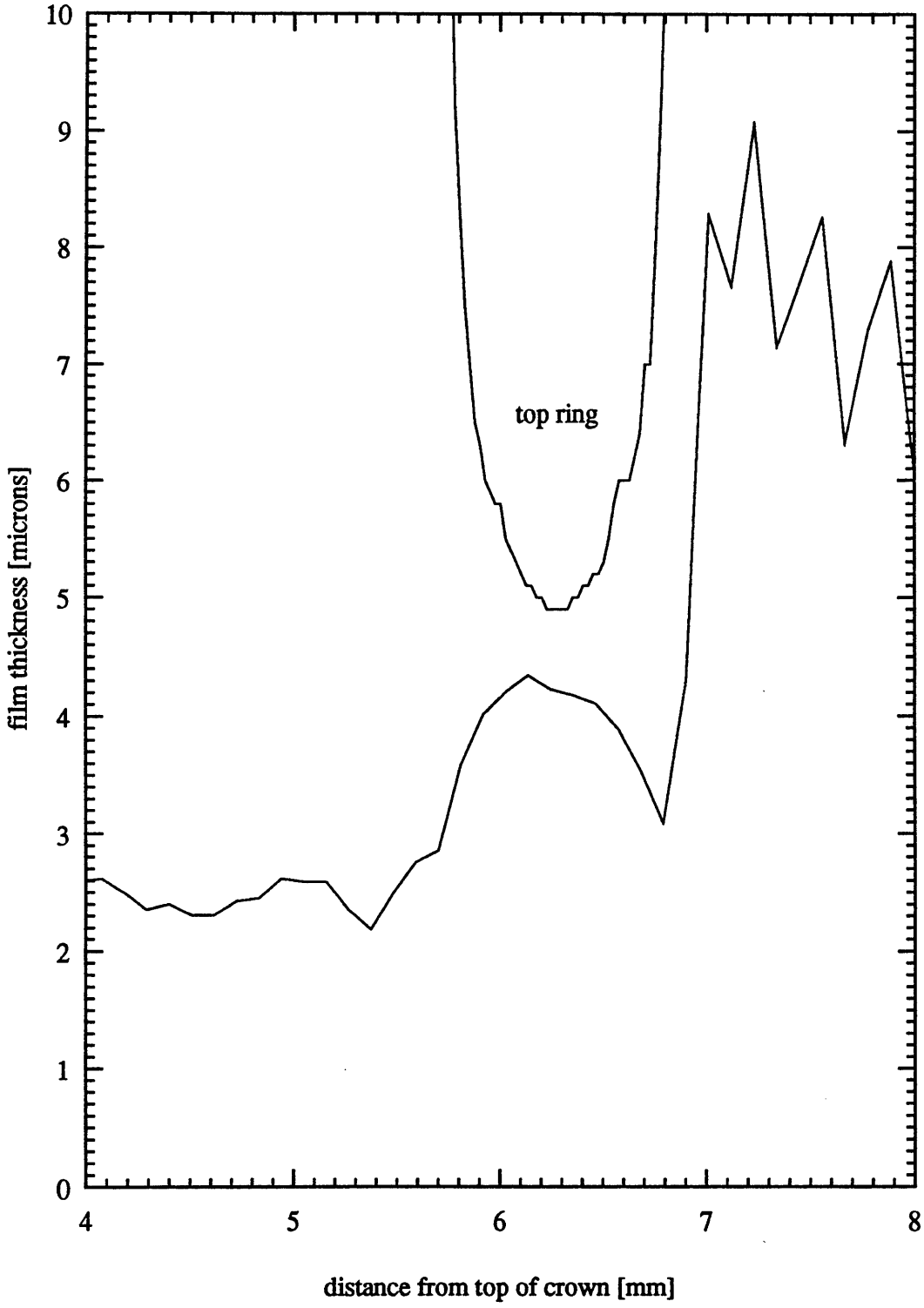

Figure 3-5 Typical difficulty with ring fit. OIL-5, 2500 rpm, 20 N-m load, compression stroke, averaged trace.

friction results can be generated. However, there is no experimental measurement of wetting variables or ring friction to confirm the theoretical predictions.

3.6 Reading h_∞ and h_0 from the Averaged Film Traces

After a data set for a particular oil and running condition has been calibrated using the method described in section 3.3 above, an averaged data set, which is the average of the LIF signal from twenty engine cycles, is imported into the LIF data analysis spreadsheet. The film traces in the top ring region were not found to vary significantly from cycle to cycle so that a meaningful averaged trace may be obtained in which some of the noise in the signal is removed. The smoother traces provide a better surface against which to place the ring profile. For the purpose of ring fitting, individual (not averaged) traces were also tried but without success.

Figure 3-6 illustrates the technique of reading h_0 from the averaged oil film trace. The segment of the trace between 4 and 8 mm from the top of the piston is expanded to exhibit the details of the top ring oil film. The top ring profile, obtained from a Talysurf profilometer instrument, is positioned for best possible fit on the oil film. The minimum film thickness under the ring is recorded as h_0.

Figure 3-7 shows the portion of the film trace from which the oil film thickness above the top ring, h_∞, is read. From the jump in film thickness at zero on the x-axis, this trace appears to have about a micron of oil on the crown even though it is from a fired running condition. The LIF spreadsheet has a provision for obtaining the average film thickness in the region above the top of the piston crown (from -10 to -2 mm on Figure 3-7), or, more accurately, during the time just before the top of the piston passes in front of the laser beam. This film thickness value is recorded as h_∞.

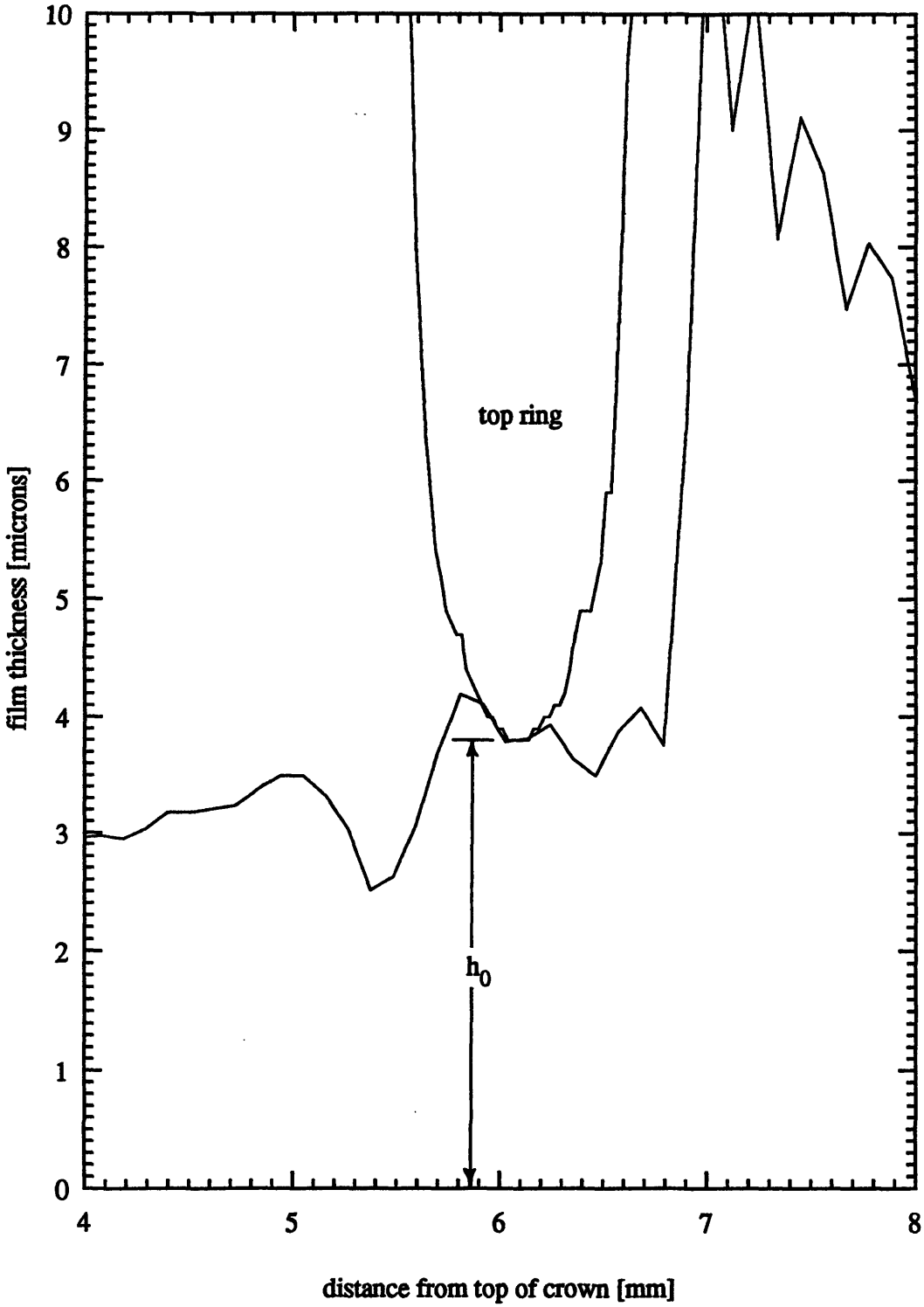

Figure 3-6 Example of h_0 measurement. OIL-8, 2500 rpm, 20 N-m load, compression stroke, averaged trace.

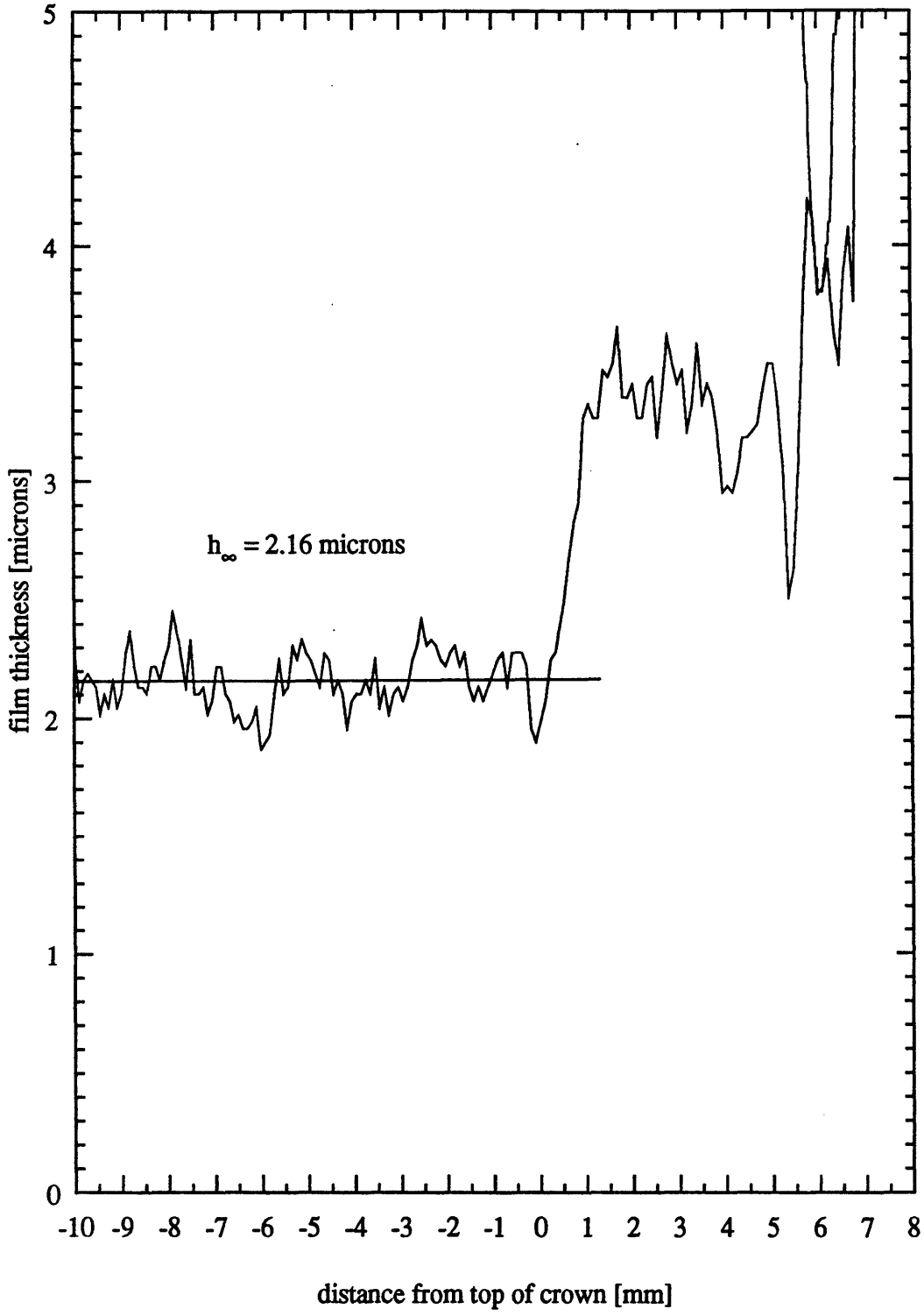

Figure 3-7 Example of h_∞ measurement. OIL-8, 2500 rpm, 20 N-m load, compression stroke, averaged trace.

CHAPTER 4: Analysis of Film Thickness Data

4.1 Comparison with Diesel Engine Data

Oil film behavior in the Kohler gasoline engine is broadly similar to that in diesel engine data taken in the past. The rings appear as depressions in the film thickness trace, and machining marks appear as jagged contours. As in the past the piston crown generally runs with a thin oil film when motored and dry when fired, leading to the conjecture that combustion burns oil off the crown land or that high cylinder pressure pushes oil down toward the crankcase. As in the fired film traces of Lux [5] the greatest accumulations of oil appear near the OC ring, and the distribution of oil on the second and third lands is generally similar to Lux's diesel. Also, skirt film thicknesses for the Kohler engine are in the same range (25 to 100 microns) as for Lux's Cummins VT-903 SCE. The Cummins engine OC ring rails rode on films about 15 microns thick as do the OC rails in the present Kohler engine. A further similarity is the observation that top and second ring oil films are much thinner (one-third to one-fifth as thick) than OC ring films.

The ratio of h_∞ to h_0 obtained in this work is in the range 0.5 to 0.7. These values, which are less than one, are similar to those found in past work at M.I.T. Thus the wetting phenomenon is consistent with prior observations. A sub-ring oil flow with h_∞/h_0 near 0.5 means the ring is running in a starved condition. Mass conservation dictates that 0.5 is the theoretical lower limit for h_∞/h_0. Since Azzola's computer model is based on the starved flow assumption, the code should be applicable to the present data. Chapter 5 covers the use of Azzola's computer model to calculate drag.

There is only one significant deviation of the present data set from the character of the diesel film traces. While Lux saw higher peak film thicknesses in the OC ring

region for the gas exchange revolution than for the power revolution in fired data, the present data shows no such trend. Lux observed that local OC ring oil films were thicker on exhaust and intake strokes than on compression and expansion strokes. The Kohler engine data exhibits little differentiation with respect to gas exchange versus power revolutions but does seem to segregate by upstrokes versus downstrokes. The detailed behavior of the Kohler film traces is covered in the following section.

4.2 Details of the Kohler Engine Data

Figure 4-1 displays typical oil film traces from motored data as the piston passes by on intake, compression, expansion, and exhaust strokes. Each trace is the average of twenty consecutive strokes from the same data set. The engine speed is 1800 rpm. The cycle-to-cycle variability is approximately 10% in this data.

The motored traces show marked differences between upstrokes and downstrokes. The intake and expansion strokes (downstrokes) exhibit large spikes of oil just below each of the OC ring rails. These peaks are about 100 to 200 microns in magnitude. The films on the piston skirt are between about 20 and 40 microns thick for these downstrokes, which agrees with the measurements of Lux [5]. By contrast, the compression and exhaust strokes (upstrokes) exhibit less salient spikes below the OC rails and have thicker skirt films--in the range of 30 to 90 microns.

The sloping nature of the upstroke skirt films in the region 20 to 30 mm from the top of the crown may be due to the barrel shape of the piston skirt, to motion of the piston within the bore, and/or to elastic deformation of the skirt. The difference in radius between the narrow top (20 mm from top of crown) and wide middle (30 mm from top of crown) of the skirt profile is about 75 microns, which is about the same as the change in thickness between those two points on the film trace.

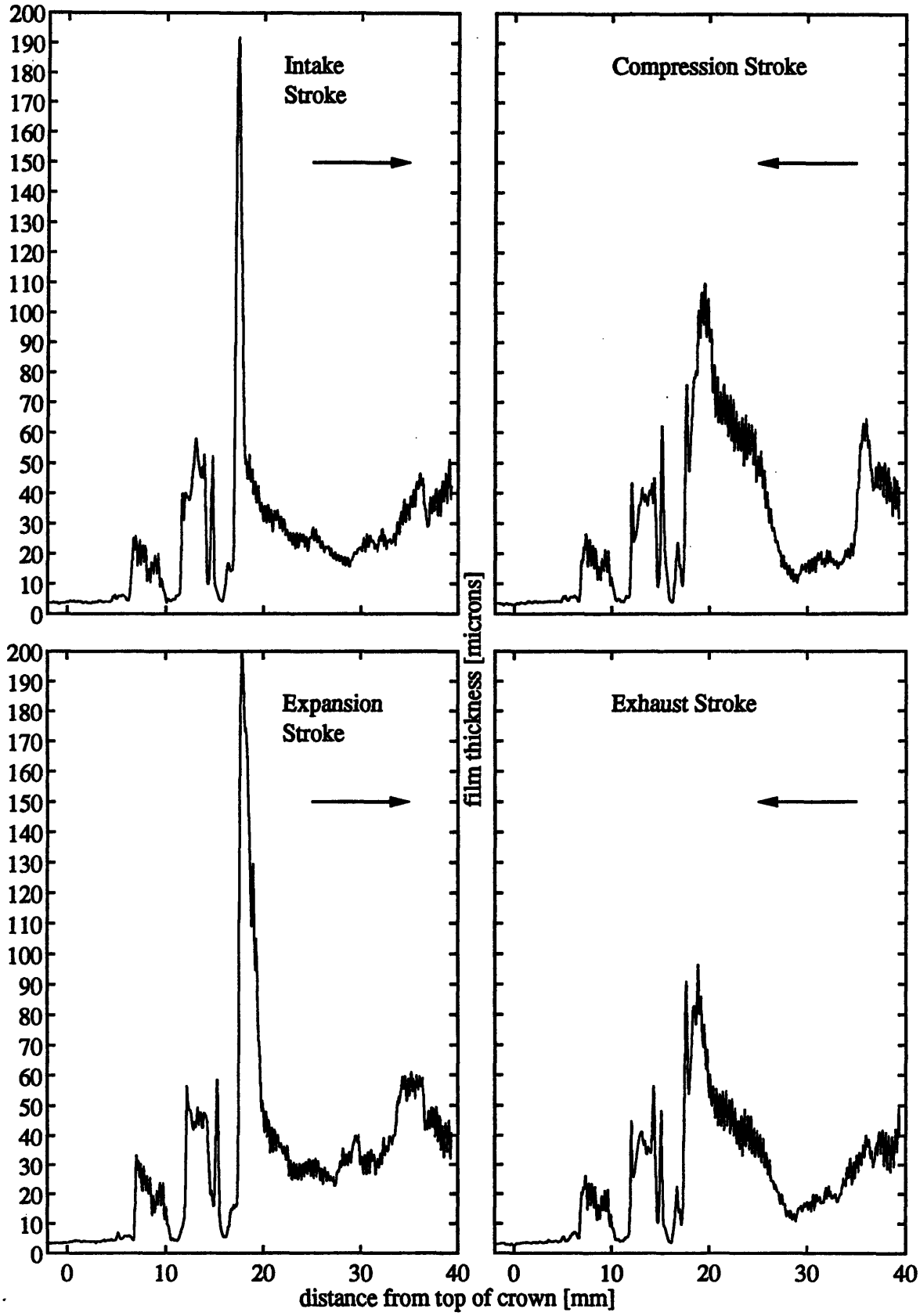

Figure 4-1 Averaged film thickness traces for four strokes. Running condition: motored at 1800 rpm. Arrows indicate direction of piston travel.

Note that it is unlikely that oil completely fills the space between the piston skirt and liner at all times, so the possibility of gaseous voids should be taken into account when viewing the film traces. The LIF system does not respond to gas, only to dyed oil (see section 3.2 Interpreting a Film Trace). Therefore, if during the intake stroke the piston/liner clearance is not fully filled with oil, the measured film thickness variation will be different from the skirt profile variation.

The oil film behavior for the regions above the OC ring--the crown, the top and second rings, and the second and third lands--is largely similar for all four strokes. Noteworthy is the small lump of lubricant just above the top ring (about 4.5 mm from the top of the crown) which is absent in fired traces. Since the end of the lump coincides with the top edge of the top ring groove (which is also the bottom edge of the piston crown), it is likely that this lump is a small accumulation of oil on the piston crown surface rather than on the cylinder liner. Therefore, the lump may not be related to top ring lubricant flow.

Typical film traces from fired data are presented in Figure 4-2. The engine speed is the same as for the motored traces in Figure 4-1 (1800 rpm) while the fired load torque is 10 N-m. Comparing motored and fired conditions, the top ring oil film is generally thicker in motored data than in fired data. The scale of Figures 4-1 and 4-2 is not expanded to properly view the top ring area, but enlargements of that part of the film trace (see Figure 4-3) show that minimum film thickness under the top ring is around 5 to 6 microns in motored data and around 2 to 4 microns in fired data. The occurrence of thicker films under motored conditions may be due to the presence of cooler, thicker oil around the ring pack or to the lack of combustion-induced oil burn-off.

Aside from the film thickness difference between motored and fired conditions, the general character of the film traces remains the same. There are some differences in

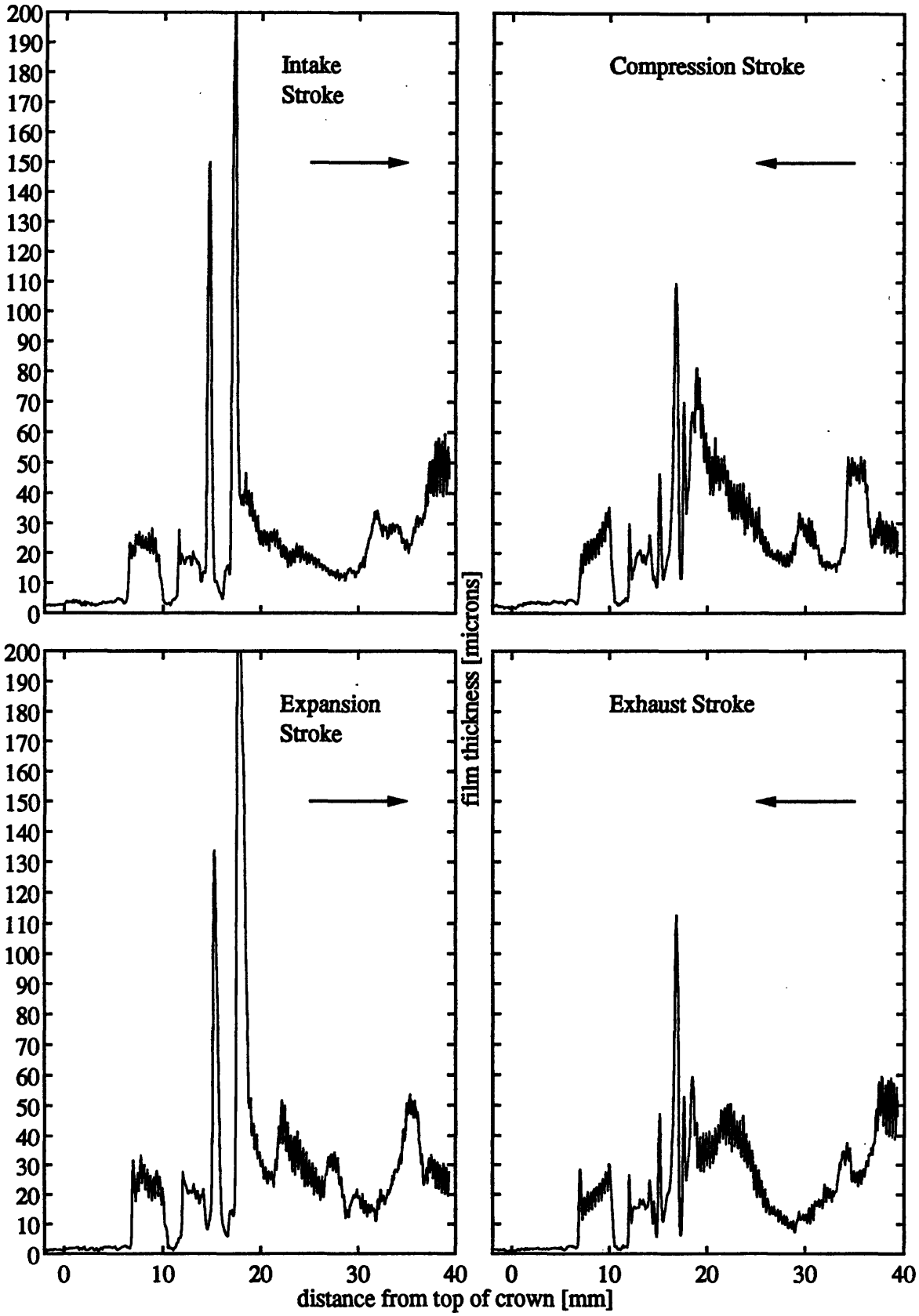

Figure 4-2 Averaged film thickness traces for four strokes. Running condition: fired at 1800 rpm and 10 N-m load. Arrows indicate direction of piston travel.

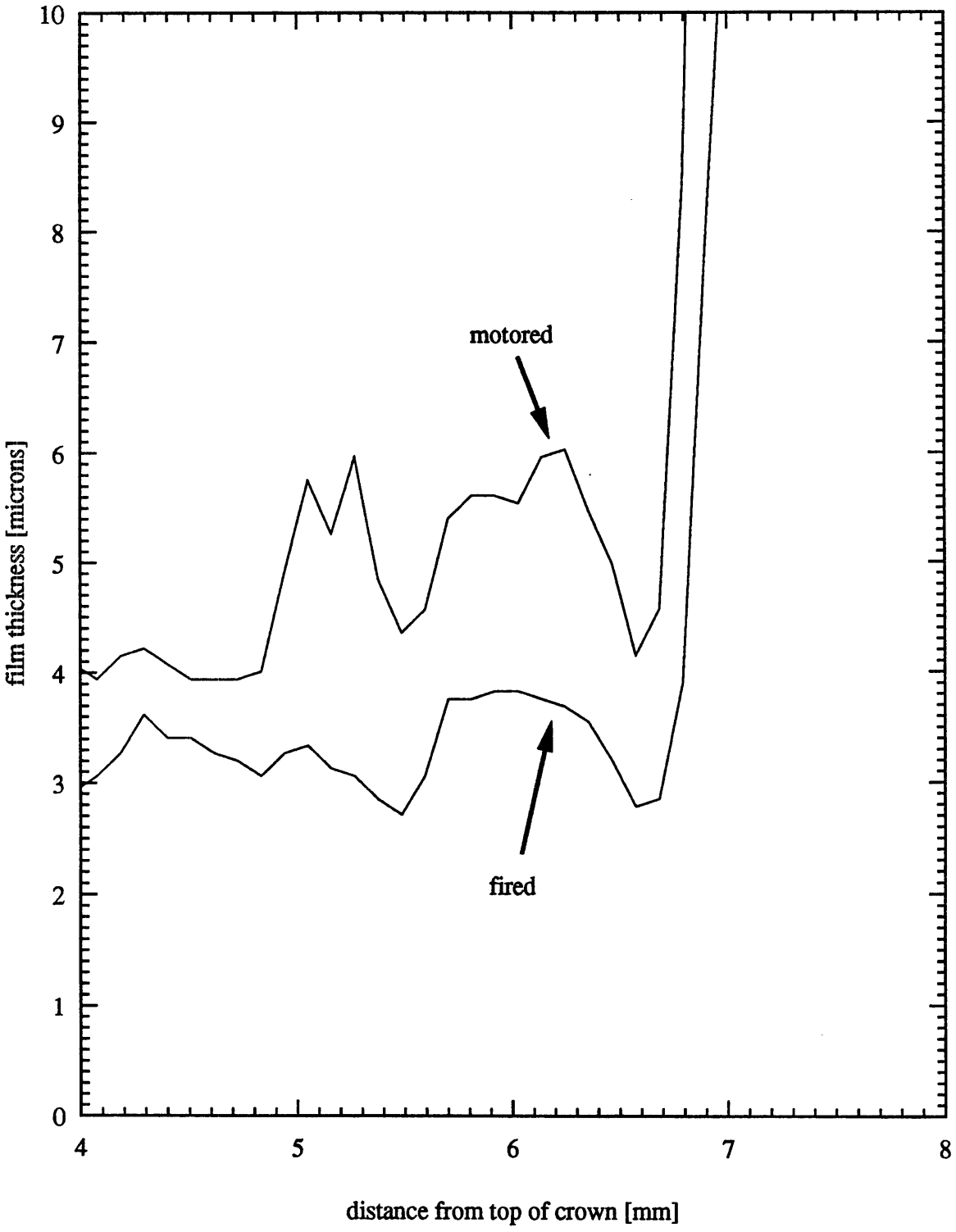

Figure 4-3 Top ring oil film trace for motored and firing engine conditions.
1800 rpm, compression stroke, averaged trace.

the overall shape of the second land and skirt oil films, but these differences could be due to differences in piston motion or to random variations in film behavior between data sets.

4.3 Observations About h_∞ and h_0

The primary observation about oil films around the top ring is that in fired data, expansion and exhaust stroke oil films are less thick than intake and compression stroke oil films. Figure 4-4 illustrates this phenomenon with top ring oil film thicknesses from four consecutive strokes of the firing engine. In motored data, no such difference between film thickness on different strokes exists. The combustion event seems to exert some influence on measured film thickness.

Since temperature is known to affect the LIF calibration coefficient, it was speculated that combustion might heat up the oil film enough to degrade the local LIF calibration coefficient. However, a heat transfer calculation revealed that the small temperature rise (about 1 degree C) in the oil film due to combustion heat release could account for only a fraction of a percent change in calibration coefficient, not for the observed 30 percent drop in LIF signal from compression to exhaust strokes. The mechanism which governs this lowering of signal on expansion and exhaust strokes is not known.

Brown, McCann, and Thompson at Shell Research Ltd. [9] saw the same drop in signal during expansion and exhaust strokes. They speculate that localized heating of the oil film under the top ring causes an apparently thinner film to be detected because of a locally changed LIF calibration coefficient. Given a highly elevated top ring temperature, this explanation is plausible.

A second observation on the nature of h_∞ and h_0 data is its trend with viscosity and surface tension. The h_∞ values for oils of varying surface tension but nearly

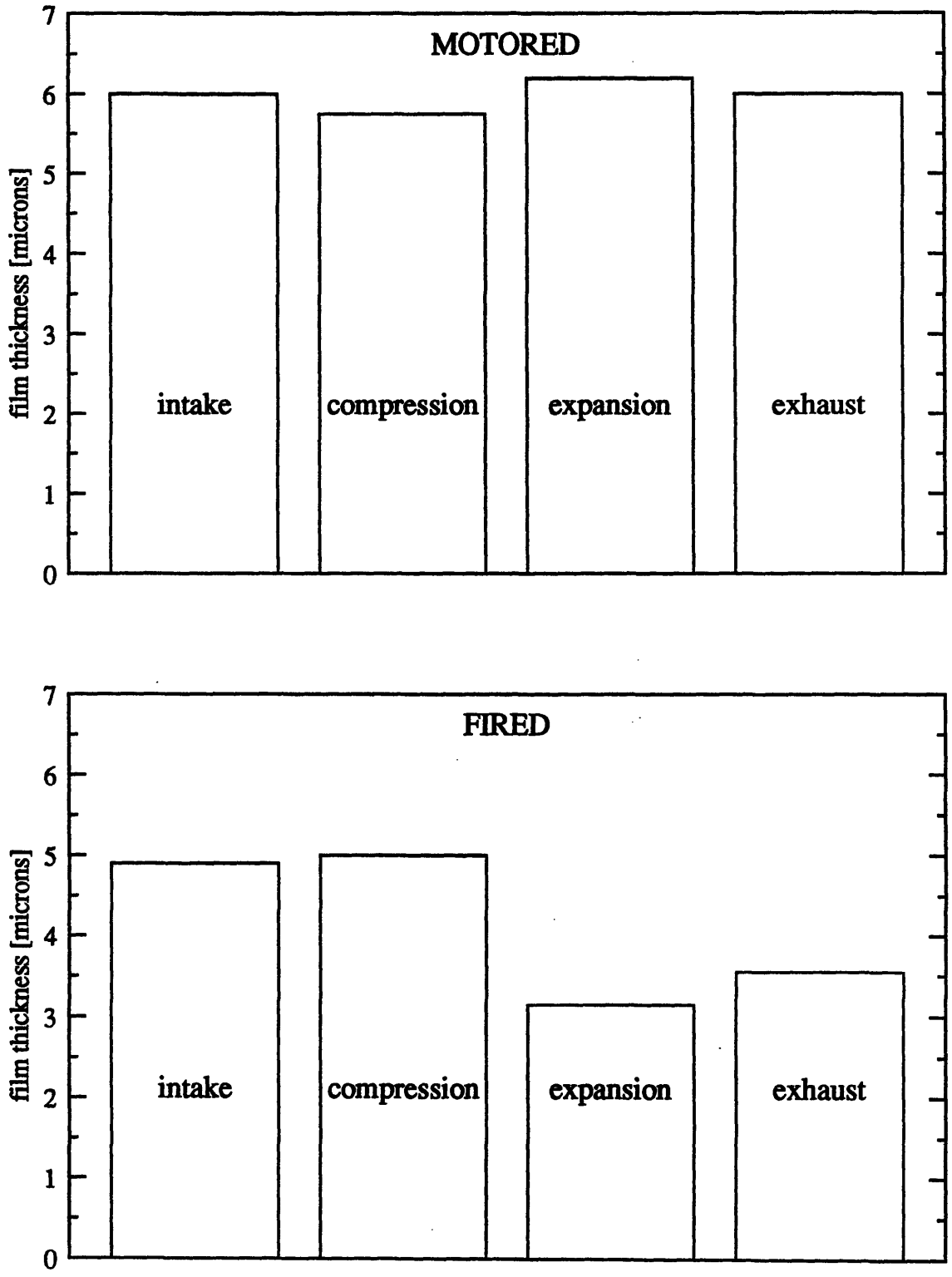

Figure 4-4 Minimum film thickness under top ring for four consecutive engine strokes under motored and fired conditions. Fired strokes show drop in film thickness on expansion and exhaust strokes. OIL-C, 2500 rpm, averaged data.

constant viscosity are displayed in Figure 4-5 for a particular running condition. The h_0 and h_∞ values for oils of varying viscosity are displayed in Figure 4-6, but these oils (OIL-A through F) vary in surface tension as well as in viscosity. The trends for h_0 follow those for h_∞ since the ratio h_∞/h_0 remains nearly constant throughout the data. In broad terms, h_∞ and h_0 seem to decrease with increasing viscosity and surface tension. This trend becomes important when interpreting the results of the Azzola ring friction computation.

For fixed h_∞, Azzola theory predicts that friction decreases with increasing surface tension, but the present data has widely varying h_∞. The variation in h_∞ gives rise to a competing mechanism affecting friction. Thus there are two mechanisms affecting friction. 1) The Azzola model with fixed h_∞ asserts that a surface tension increase causes wetted width to decrease, causing friction to decrease. 2) The experimental observation about h_∞ variation shows that a surface tension increase causes h_∞ to decrease, causing h_0 to decrease, in turn causing friction to increase. Therefore, an increase in surface tension can cause engine friction to increase, decrease, or stay constant, depending on which mechanism dominates. Section 6.4 contains a detailed explanation of the Azzola mechanism for friction reduction.

The researchers at Shell found a similar relationship between film thickness and viscosity for their low speed and load running conditions; i.e. they saw thinner films at higher viscosity. It is possible that a high-viscosity lubricant has a harder time getting to the upper part of the cylinder liner, resulting in low film thickness. The Shell researchers explain: "The relative film thickness behaviour of the two lubricants at low temperatures (low engine speed and torque conditions) may simply be a function of the easier transport, or 'pumpability', of the lower viscosity grade lubricant such that inherently larger amounts are available for supply to the liner and for subsequent transport through the ring pack" [9].

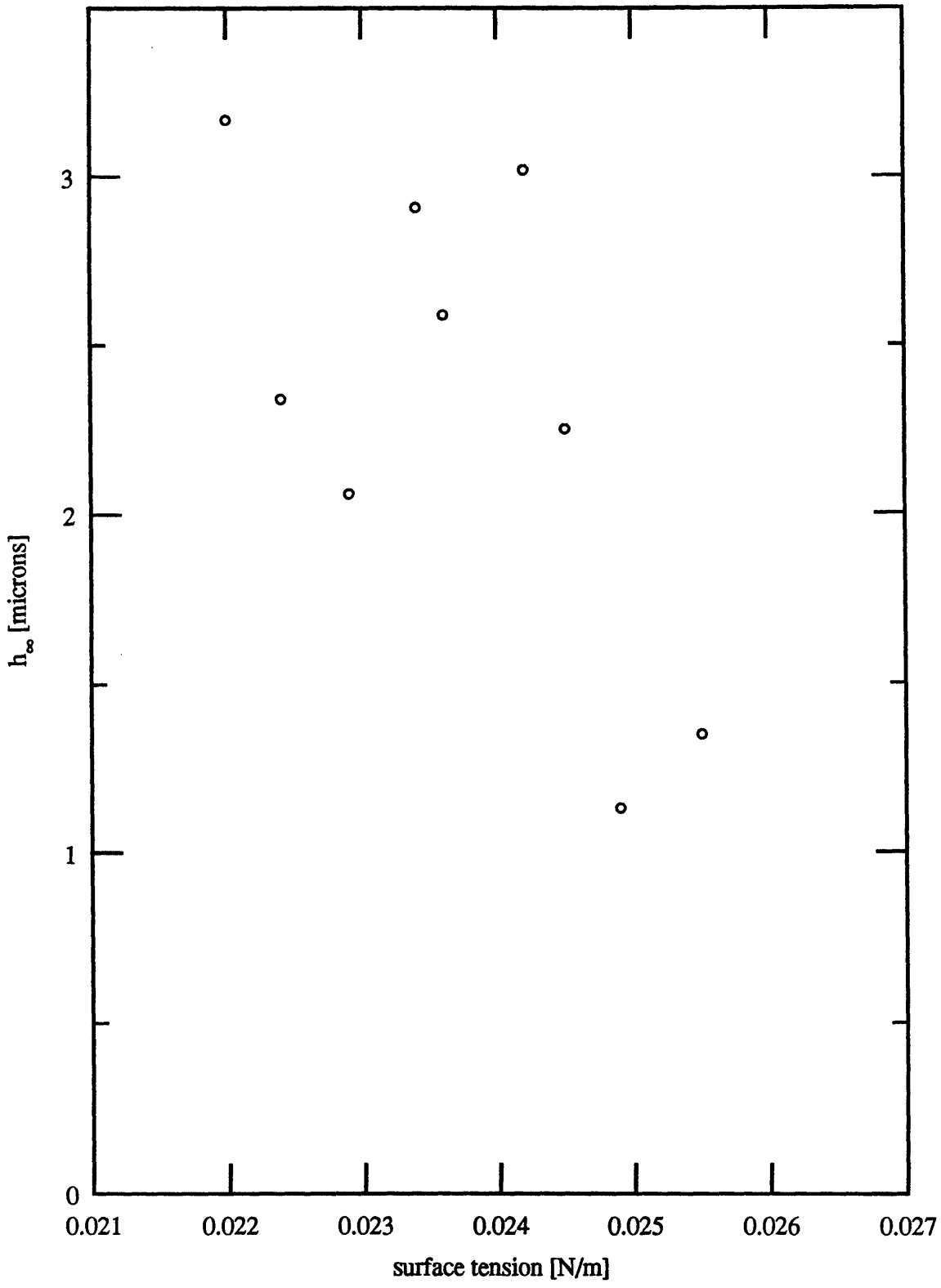

Figure 4-5 h_∞ versus surface tension for oils of similar viscosity. Running condition: 2500 rpm, 20 N-m load, 100 °C.

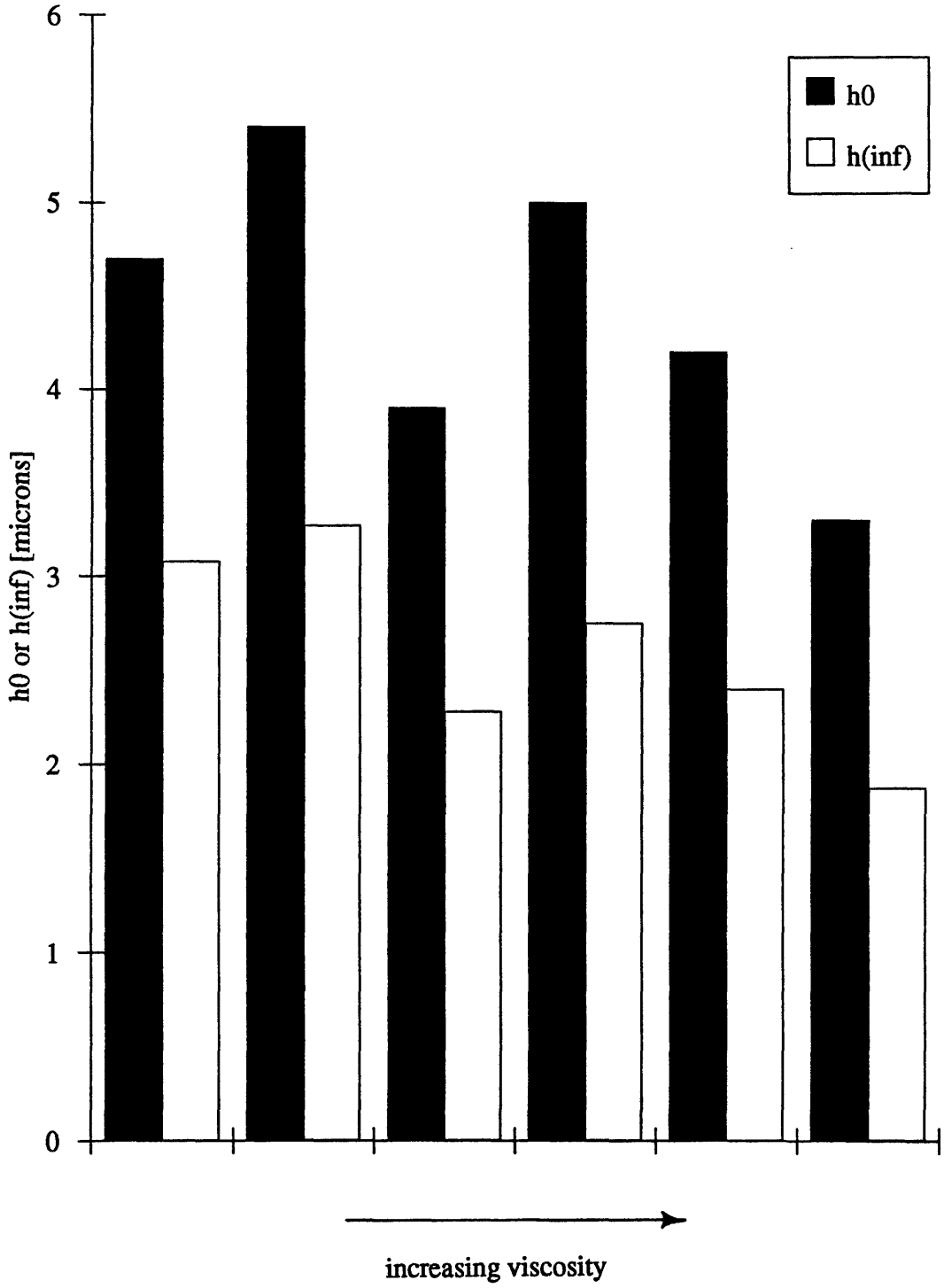

Figure 4-6 h_0 and h_∞ for oils that vary in viscosity and surface tension. Running condition: 2500 rpm, 20 N-m load, 100 °C, compression stroke.

The third observation about h_∞ and h_0 involves the ratio of h_∞ to h_0 and has been covered in section 4.1.

4.4 Speed and Load Effects on Film Thickness

The effect of engine speed on top ring film thickness can be seen from an 1800 versus 2500 rpm speed comparison at motored and 10 N-m load conditions: On the compression stroke at motored conditions, averaged (across all the oils) h_0 is 5.33 microns at 1800 rpm and 5.76 microns at 2500 rpm; so there is an insignificant increase in thickness with increasing speed. On the compression stroke fired at 10 N-m load, averaged h_0 is 3.52 microns at 1800 rpm and 3.32 microns at 2500 rpm; that is, film thickness actually went slightly down with increasing speed. Figure 4-7 illustrates these film thicknesses. The Shell researchers also found that film thickness under the top ring is largely independent of speed, but their liner temperature floated whereas the Kohler liner temperature was kept constant at 100 degrees C for all fired cases.

The effect of load on film thickness is shown by a low versus high load comparison at 1800 and 2500 rpm: For the compression stroke at 1800 rpm, averaged h_0 is 3.08 microns at 5 N-m load and 3.52 microns at 10 N-m load; that is, film thickness went up with increasing load. For the expansion stroke at 1800 rpm, averaged h_0 is 2.03 microns at 5 N-m load and 2.25 microns at 10 N-m load. For the compression stroke at 2500 rpm, averaged h_0 is 3.32 microns at 10 N-m load and 4.06 microns at 20 N-m; once again, it went up with increasing load. For the expansion stroke at 2500 rpm, averaged h_0 is 2.23 microns at 10 N-m load and 2.71 microns at 20 N-m load. These film thicknesses are presented in Figure 4-8. The Shell results compare favorably with these results for certain running conditions.

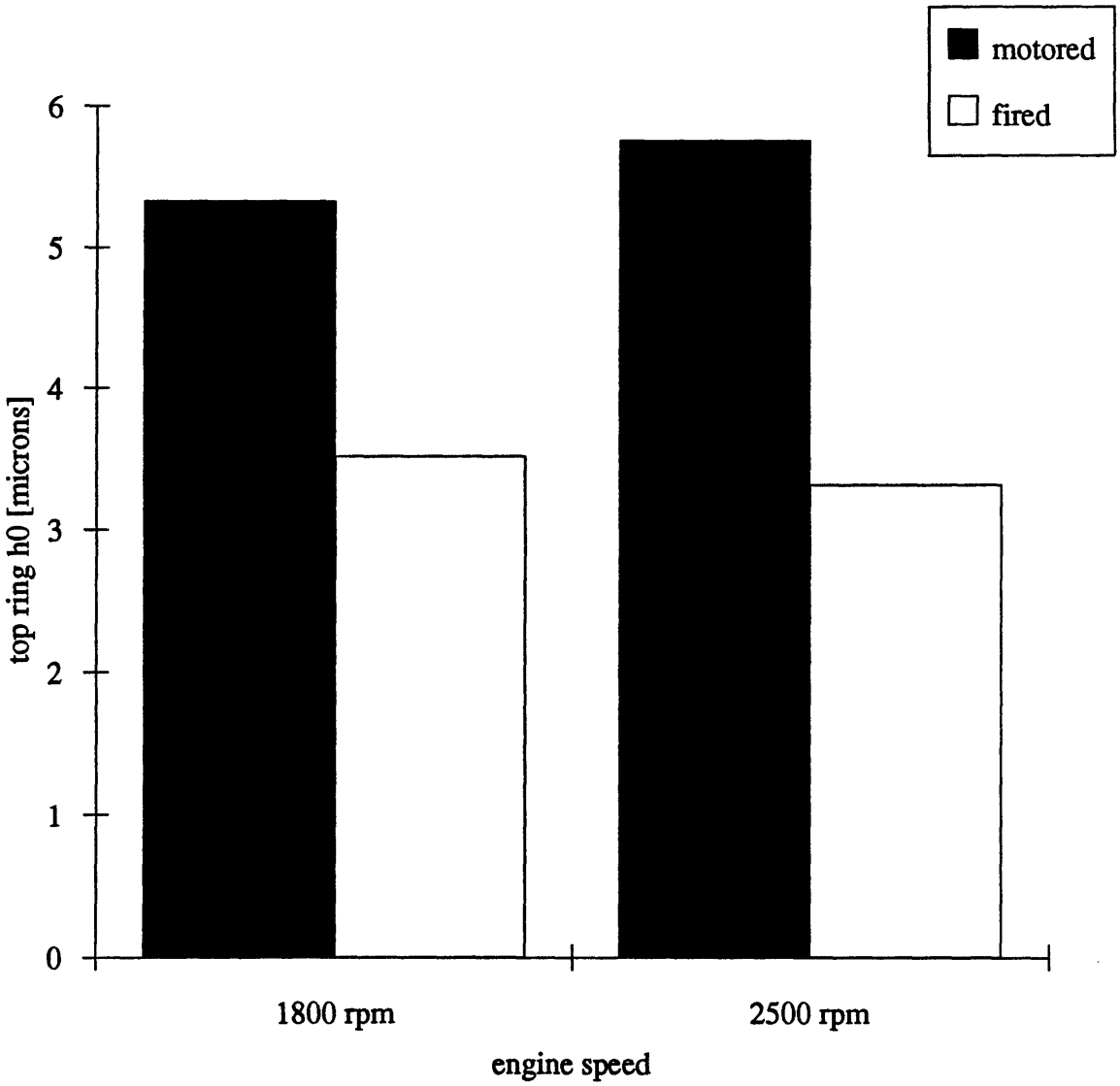

Figure 4-7 Speed comparison of average (across all oils) top ring film thickness for motored and fired (10 N-m load) conditions, compression stroke. Note that film thickness is relatively independent of speed.

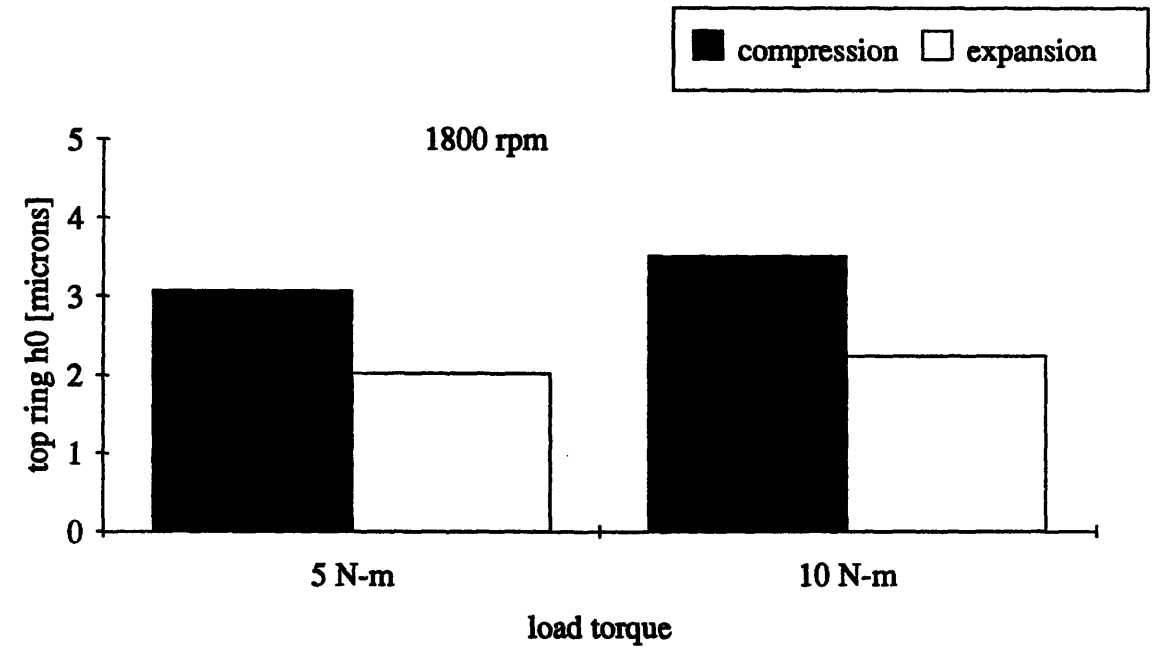

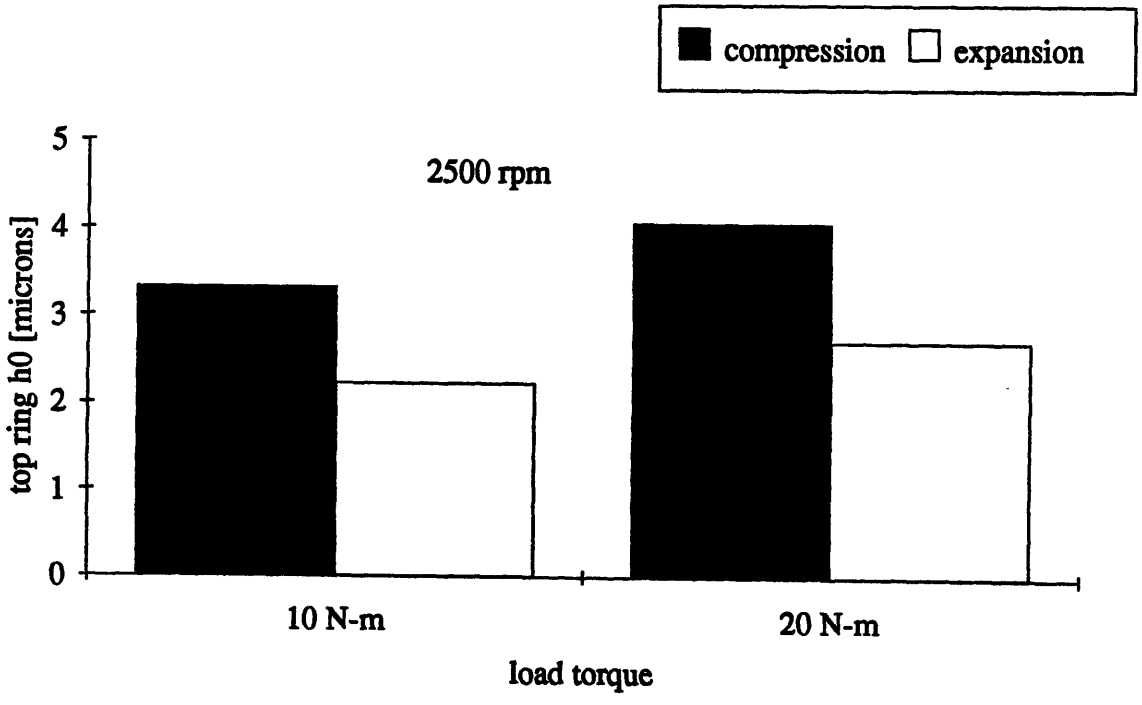

Figure 4-8 Load comparison of average (across all oils) top ring film thickness for 1800 and 2500 rpm, compression and expansion strokes.

CHAPTER 5: Top Ring Wetting and Friction Model

5.1 Relevance to Project

Since a friction comparison between oils was the impetus of the data analysis, a computer model of top ring oil flow was used to calculate friction based on film thickness measurements. The theoretical model will be described, then the exit boundary condition. The structure of the code will be explained. Finally, the friction results will be discussed along with some of the deficiencies in the analysis.

5.2 Description of the Model

The computer model of top ring lubricant flow was developed by Dr. James Azzola in his Ph.D. thesis [2]. The model is essentially Newtonian in nature with the addition of a novel exit boundary condition. The basis of the code is the simplified two-dimensional Navier-Stokes equation for steady state (no squeeze film term) hydrodynamic viscous flow:

$$\frac{d}{dx}\left(\frac{h^3}{\mu}\frac{dP}{dx}\right)=6U\frac{dh}{dx} \qquad (5.1)$$

also called the Reynolds equation for lubricant flow. For the purpose of the mathematical analysis, the top ring/cylinder liner is idealized as a circular slider bearing. The Reynolds equation is integrated to solve for the sub-ring pressure distribution and hydrodynamic lift force.

The details of non-dimensionalization and equation manipulation are covered in the Azzola thesis [2]. There are three equations: 1) calculated pressure difference

across the ring equals input P_1 minus P_2 (variables are defined in the nomenclature section), 2) hydrodynamic lift force (from integration of the pressure distribution) equals imposed ring load (sum of pressure loading and elastic tension), and 3) shear stress equals surface tension gradient at the film detachment point (the exit shear stress boundary condition). These equations are used to solve for the three unknowns: h_∞, x_1, and x_2.

Actually, there are two versions of the code. The one explained in this chapter takes h_0, oil properties (μ and σ), engine conditions (U, P_1, and P_2), and ring parameters (L, a, and B) as input and calculates h_∞, x_1, and x_2. The other, employed in the parametric study of Chapter 6, takes h_∞, oil properties, engine conditions, and ring parameters as input and calculates h_0, x_1, and x_2. Once h_0, x_1, and x_2 are known, all other wetting dimensions are determined by geometric relationships for the circular ring profile.

The crown land pressure, P_1, is known from the in-cylinder pressure measurement. The second land pressure, P_2, is calculated using a computer simulation of gas flow around the top ring. All other quantities are measured directly.

5.3 The Exit Boundary Condition

What makes the Azzola ring flow model unique is the use of an exit boundary condition based on a surface tension gradient at the free surface. The idea is that polar oil molecules undergo a surface tension increase at high rates of strain. Strain rates beneath the piston rings of a running reciprocating engine are quite high (on the order of 10^7 $s^{-1)}$ which gives rise to a dynamic surface tension nearly three orders of magnitude larger than the corresponding zero-strain value [2] (the zero-strain value is the traditional or nominal surface tension). This dynamic surface tension decreases from a high value at the film detachment point, where the strain rate is a maximum for

the free stream region, to a low value approaching the zero-strain-rate surface tension far downstream. Thus a surface tension gradient is set up on the free surface of the lubricant in the exit region. Imagine a fluid particle located at the point where the oil film detaches from the downstream side of the ring as illustrated in Figure 5-1. The net force on a fluid particle exerted by the surface tension gradient is balanced by the shear stress in the fluid caused by the passing ring.

The surface tension gradient is assumed to be a direct function of the nominal surface tension. The value of the constant of proportionality is found by an empirical correlation between wetting parameters from a prior data base of film thickness values.

5.4 Structure of the Code

The code solves for the wetting dimensions using an algorithm of nested loops. The outer loop steps upward (in the positive direction) in x_2. The inner loop steps downward (in the negative direction) in x_1. Refer to Figure 3-3 for a definition of the coordinate system. The code first chooses an x_2. Then it enters the inner loop and steps downward in x_1 until it finds the x_1 that causes the same pressure difference across the ring as the input P_1 and P_2 demand. Once that pressure difference condition is met, the code jumps back to the outer loop and checks to see if the loading condition is met by the current x_1 and x_2. The loading condition equates the hydrodynamic lift force generated by the lubricant flow with the imposed load caused by ring elastic tension and pressure forces. When the loading condition is satisfied along with the pressure condition, the solution has been found.

The exit shear stress boundary condition is worked into the inner loop that handles the pressure equation.

To cut down on computation time, the routine allows for a rough pass followed by subsequently finer passes in the numerical stepping procedure. The first pass uses a

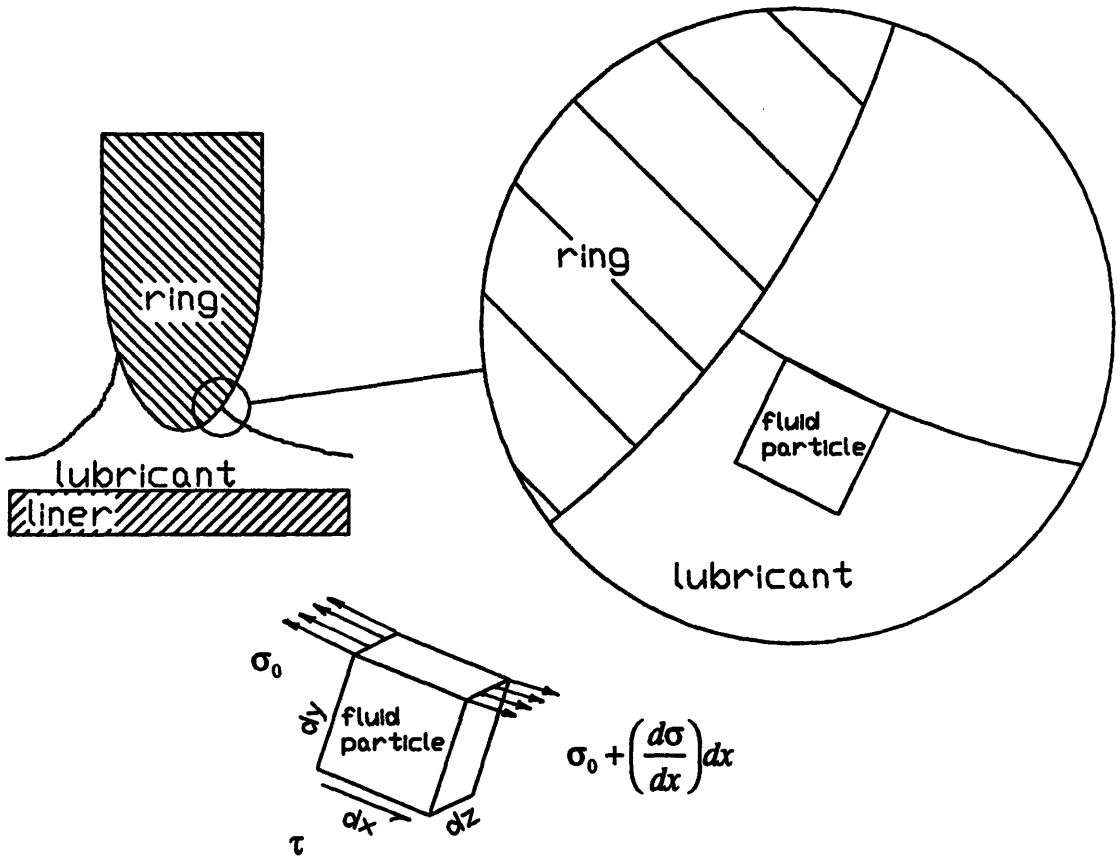

Force balance:

$$dz\left[\sigma_0 + \left(\frac{d\sigma}{dx}\right)dx - \sigma_0\right] = \tau dx dz$$

$$\frac{d\sigma}{dx} = \tau$$

Figure 5-1 Fluid particle at exit. Surface tension gradient balances shear stress.

relatively large step size to find the root crossing. Once the root is framed between two values, that interval is sub-divided into ten segments which are again tested for zero crossing. Successively finer cuts afford a high level of numerical precision.

In summary, the computer program takes the inputs: μ, σ, U, P_1, P_2, L, a, B, and h_0; and generates the outputs: x_1, x_2, h_∞. A separate set of procedures calculates friction from the wetting profile, sliding velocity, and oil viscosity.

5.5 Generating Friction Results

The model was used to calculate friction for the oils tested in order to provide preliminary estimates of ring friction. Figure 5-2 is a plot of friction values calculated from data for one of the running conditions. Bear in mind that the only film thickness input to these friction results is h_0. Trends are mostly the result of model math, not of film thickness data. The Taylor number (Ta) plotted on the abscissa of Figure 5-2 is a non-dimensional parameter equal to $\mu U/\sigma$. It is an expression of the ratio of viscous forces to surface tension forces in a flow. The Taylor number was used by G. I. Taylor to characterize the amount of liquid left on the inside of a tube after a bubble has been blown through the tube.

Since good ring fits with detailed wetting dimensions visible are rare in the data, it is impossible to verify experimentally that the model is predicting wetting accurately. Also, there is no experimentally measured friction against which to compare the calculated friction. Therefore, when viewing calculated friction values, it should be noted that there is no way to check those values--or the wetting dimensions that led to those values--against experimentally measured quantities.

The one wetting variable that can be compared against the data is h_∞. The code can be used to calculate h_∞ with experimental h_0 as input. This calculated h_∞ can be

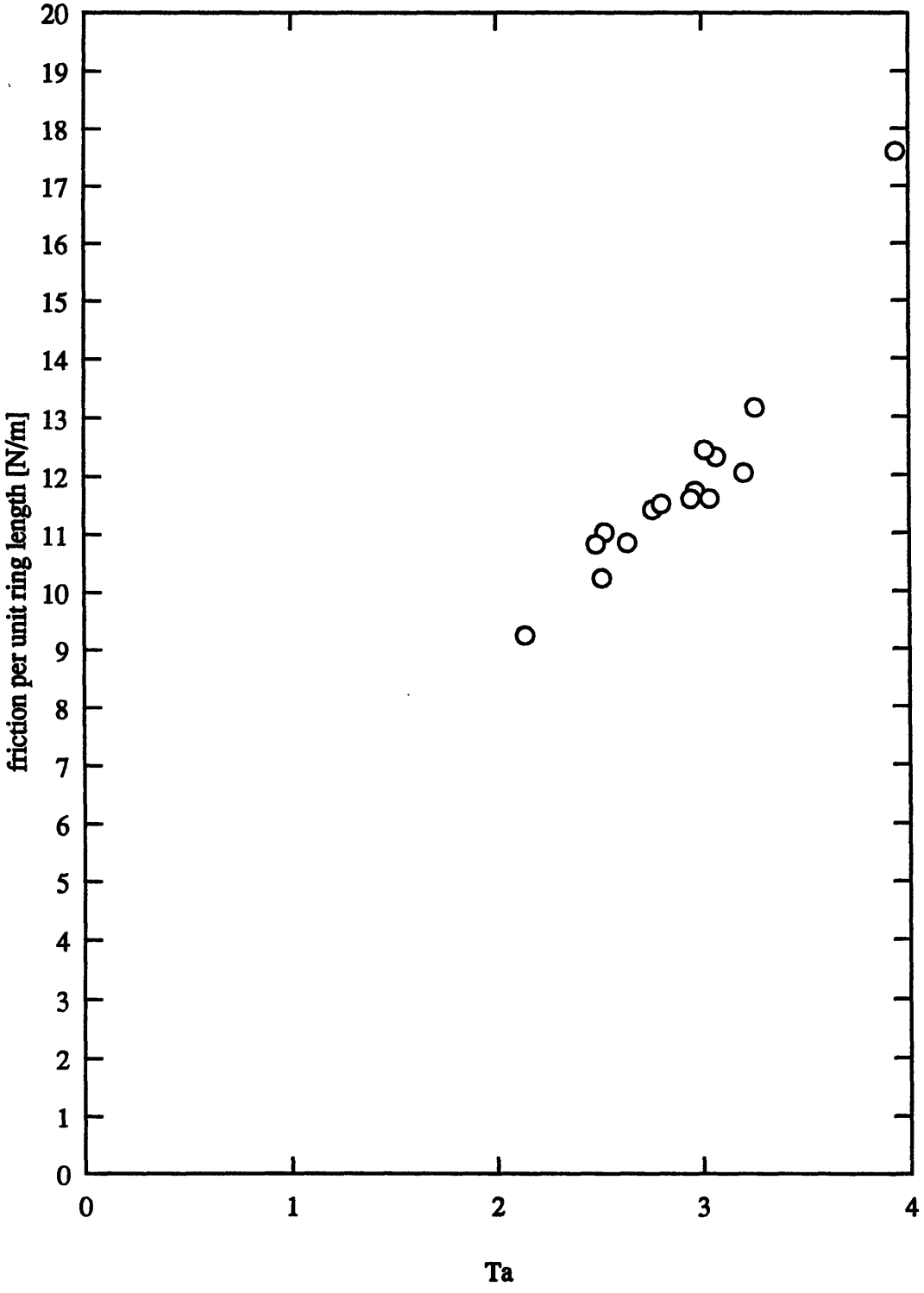

Figure 5-2 Friction versus Taylor number for all oils, 2500 rpm, 20 N-m load, compression stroke.

compared with the observed h_{∞}. Figure 5-3 illustrates the good agreement between calculated and measured values of this variable.

A deficiency in the analysis is the lack of critical experimental results to compare with the calculation results. The lack of wetting information other than h_{∞} and h_0 weakens the argument for applicability of the model to this data. A complete set of wetting dimensions from the experiment would have provided parameters against which to compare the output of the model calculation.

The ideal situation would be to see good ring fits with all wetting dimensions visible. If the results of the wetting solver code agreed with experimental wetting data, then the code could be used with confidence to calculate friction. A further check would be to compare calculated friction with experimentally measured friction. If the friction values agreed, then the code would be proven to be an realistic model of top ring lubrication. The situation just described indicates the direction for future research.

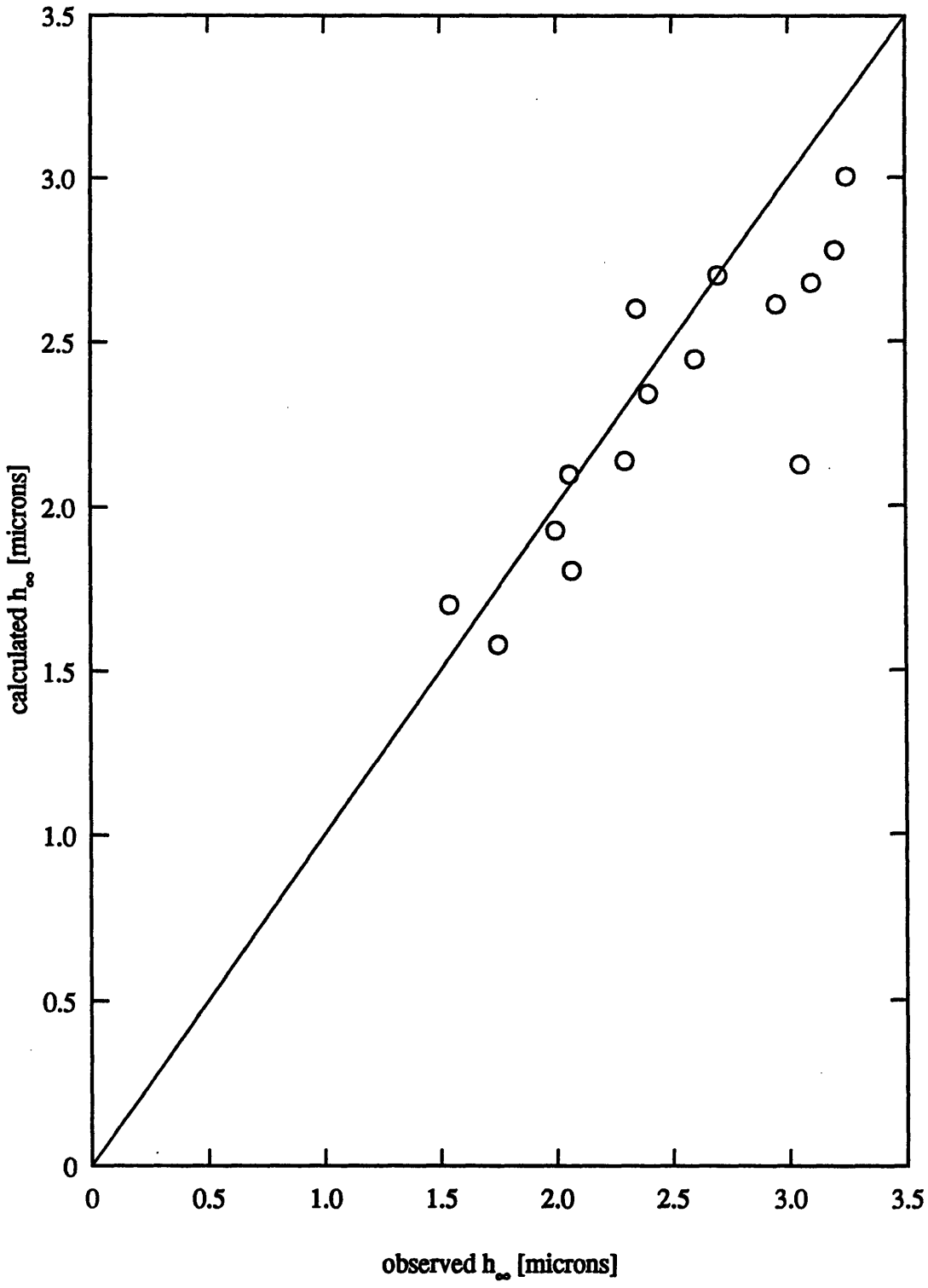

Figure 5-3 Calculated versus observed h(inf) for all oils, 2500 rpm, 20 N-m load, compression stroke.

CHAPTER 6: Parametric Study

6.1 Motivation

On the basis of the semi-empirical solution to top ring oil flow, it is of interest to know how ring friction is affected by oil properties such as viscosity and surface tension. In the following parametric study, the computer model for the top ring was used as a tool to generate curves of friction as a function of viscosity and surface tension, with all other relevant parameters held constant. The goal is to have theoretical maps showing how friction and film thickness relate to viscosity and surface tension.

6.2 Code Revision

The computer solution to the top ring lubricant flow problem was originally written as a set of macros in Microsoft Excel. The difficulties with this implementation are that Excel is not in the appropriate programming format and that the iterations run very slowly in Excel. The slowness of the code was not a problem when single cases were being run, but a parametric study demands that a batch of cases be run in order to cover a range in a variable.

The code was translated into FORTRAN with various improvements in algorithm. This version of the code takes h_{∞}, ring parameters, and engine parameters as input and returns h_0, x_1^*, and x_2^*. When the translation was finished, calculated output from the FORTRAN version was compared with output from the Excel version to ensure identical solutions from the two versions. Running in Excel, a typical data point takes twenty minutes to be solved, while in FORTRAN the same point is solved in about twenty seconds.

6.3 Calculation Method

The problem was originally posed as follows: holding h_∞ and h_0 constant (for constant wear properties--it is believed that wear is related to the oil film thickness), what is the relationship between viscosity and surface tension; and based on this functional relationship between viscosity and surface tension when film thicknesses are fixed, how does friction change with surface tension? The goal of this calculation was to determine if one can reduce top ring friction and maintain constant film thickness by tuning surface tension and viscosity. However, it was found that at a given h_∞, h_0 is nearly independent of viscosity and surface tension. For example, the calculation showed that the greatest change in h_0 over the entire viscosity range studied was only about five percent. These small changes in film thickness would not appreciably affect wear, so holding h_0 fixed was not a valid premise on which to find a relationship between viscosity and surface tension. Therefore, the purpose of the parametric study became simply to map out the effects of viscosity and surface tension on film thickness and friction as predicted by the theoretical model.

For each set of inputs, i.e., U, P_1, P_2, L, a, B, h_∞, viscosity, and surface tension, the code gives a single solution. Of the input variables, only h_∞, viscosity, and surface tension are varied. The other inputs are chosen to reflect typical Kohler engine conditions. The piston velocity of 9.07 m/s corresponds to an engine speed of 2500 rpm. The ring load of 200 N/m, ring radius of 45 mm, and ring width of 1.5 mm are all measured values for the Kohler piston top ring. In order to eliminate the effect of x_1^* and x_2^* on the ring loading balance, P_1 and P_2 are set to zero.

The first step in the calculation is to choose a nominal value for h_∞ (1.0 micron) and surface tension (0.021 N/m) and generate a curve of h_0 versus viscosity; the only varying input is viscosity. Such a curve is shown in the upper graph of Figure 6-1. The range of viscosity covered is 0.006 to 0.01 kg/m-s which spans typical motor oils. This

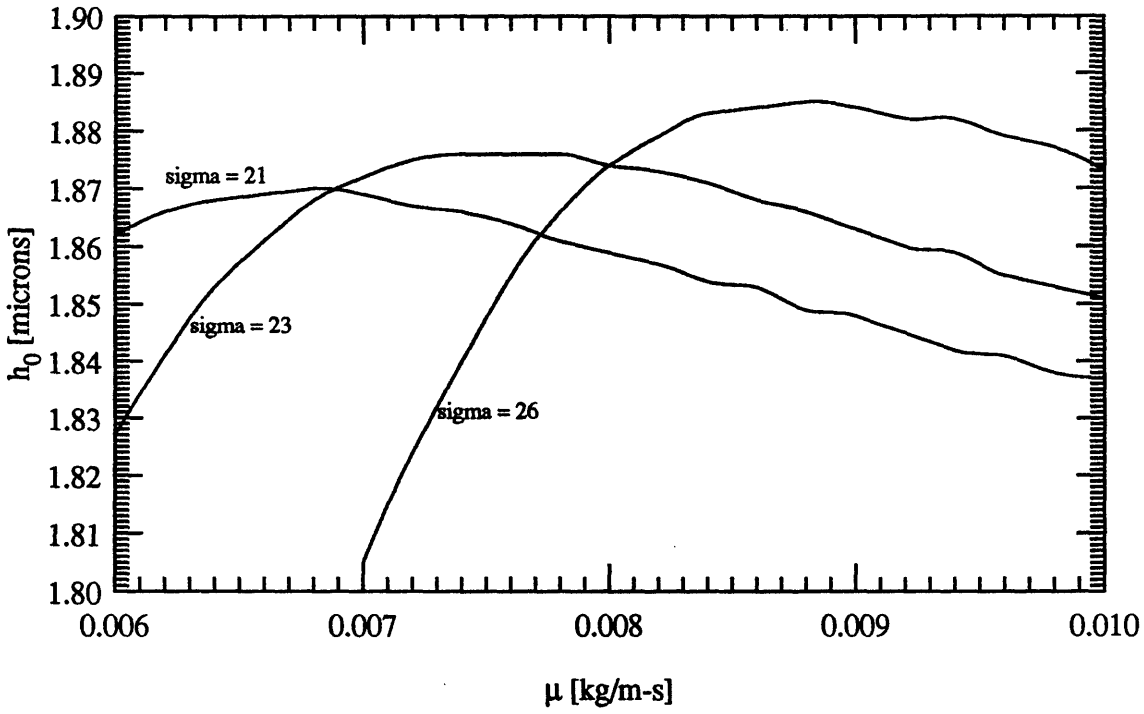

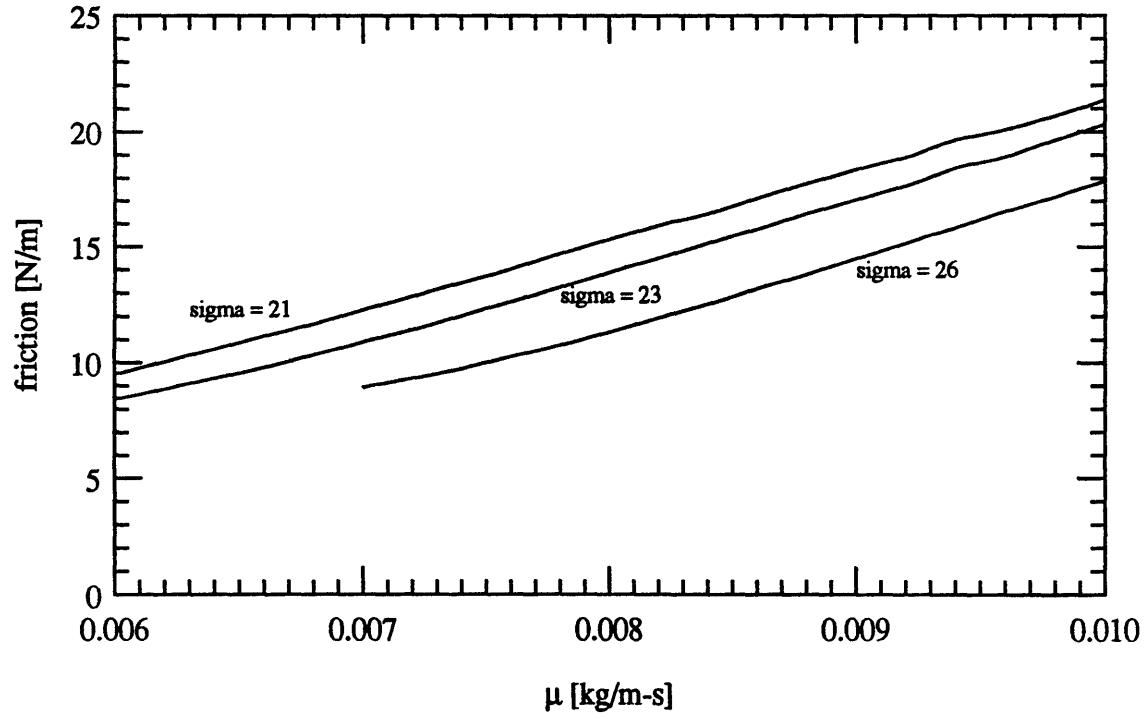

Figure 6-1 h_0 and friction vs. viscosity and surface tension, sigma [dynes/cm], for h_∞ = 1.0 micron, U = 9.07 m/s, P1 = P2 = 0, L = 200 N/m, a = 45 mm, B = 1.5 mm.

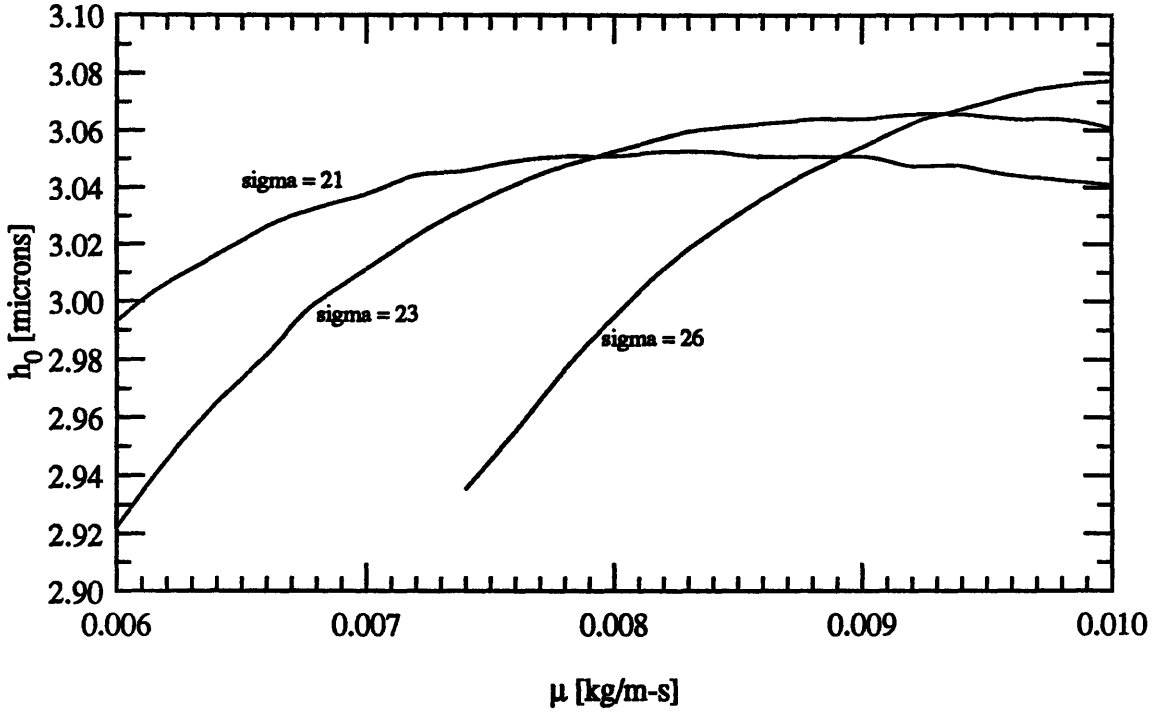

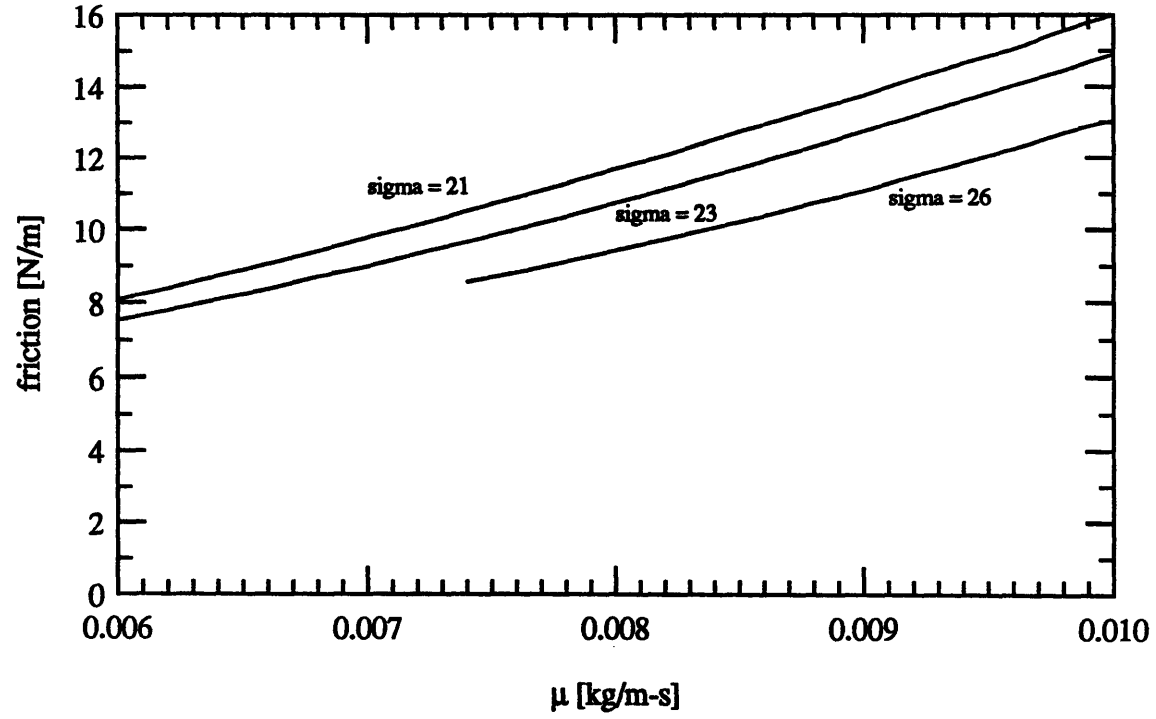

Figure 6-2 h_0 and friction vs. viscosity and surface tension, sigma [dynes/cm], for h_∞ = 1.65 microns, U = 9.07 m/s, P1 = P2 = 0, L = 200 N/m, a = 45 mm, B = 1.5 mm.

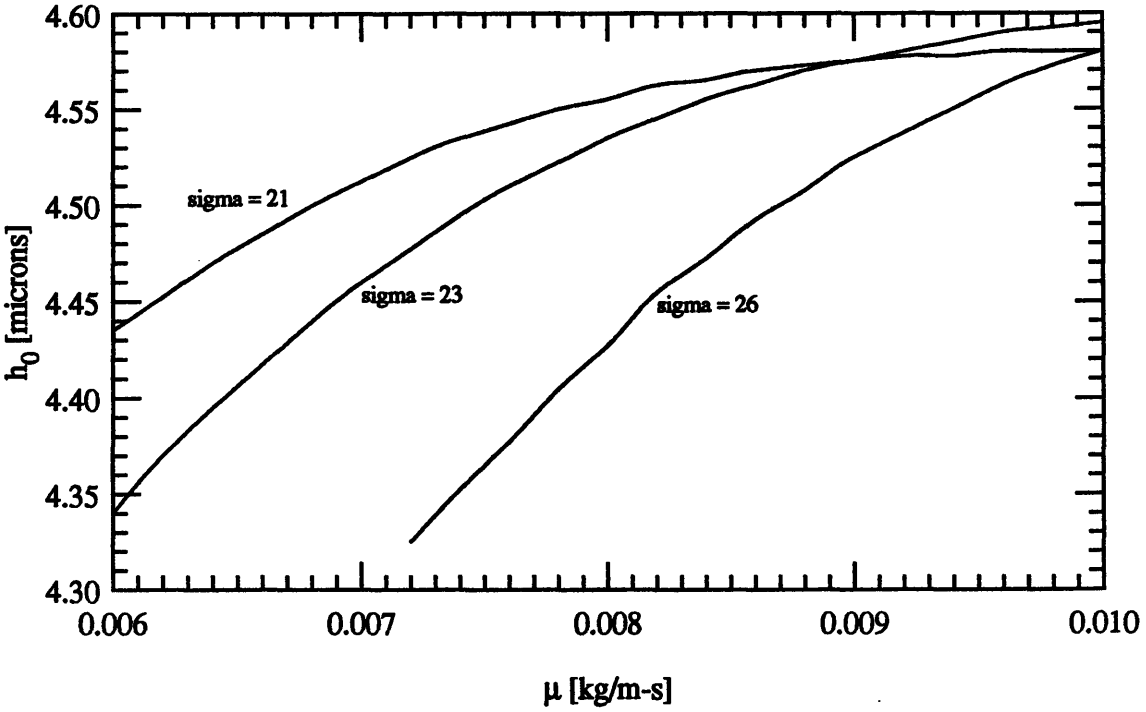

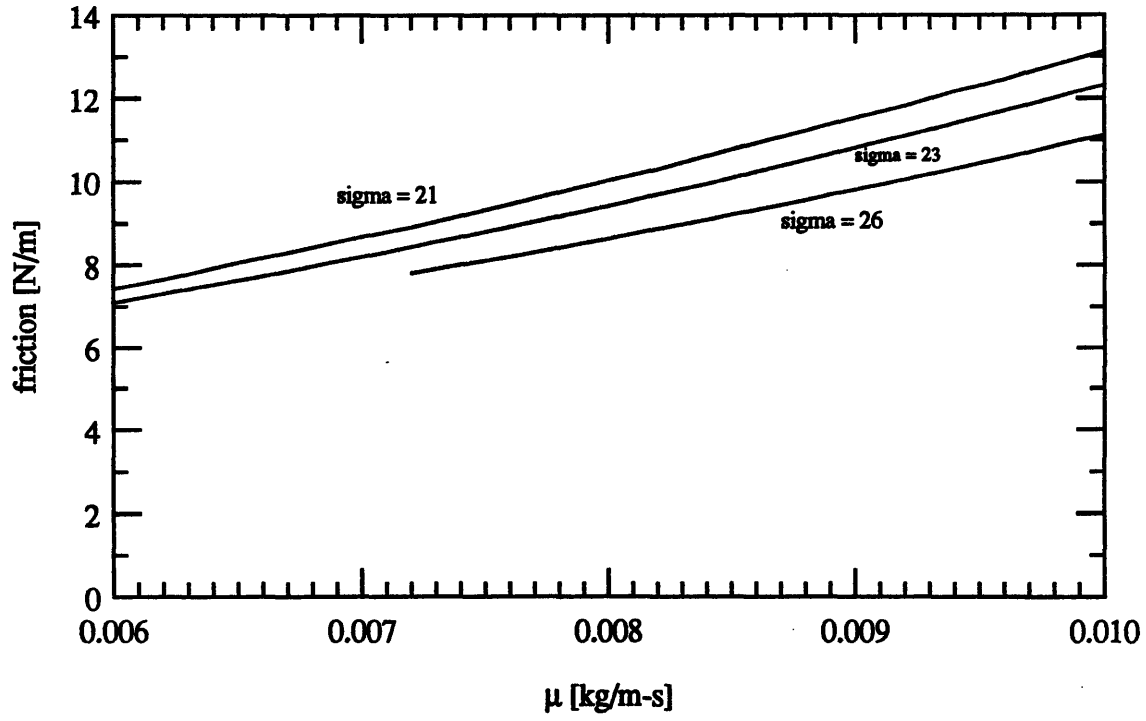

Figure 6-3 h_0 and friction vs. viscosity and surface tension, sigma [dynes/cm], for h_∞ = 2.5 microns, U = 9.07 m/s, P1 = P2 = 0, L = 200 N/m, a = 45 mm, B = 1.5 mm.

set of code-generated points shows the dependence of h_0 on viscosity alone. The h_0 versus μ calculation is repeated for two other surface tensions (0.023 and 0.026 N/m) yielding three curves of h_0 versus μ corresponding to three surface tensions. Then the entire process is repeated for two other values of h_∞ (1.65 and 2.5 microns), and the results are shown as the upper graphs in Figures 6-2 and 6-3, respectively. In the end, nine curves of h_0 versus μ are made: three surface tensions (σ = 0.021, 0.023, and 0.026 N/m) by three h_∞'s (h_∞ = 1.0, 1.65, and 2.5 microns).

Since viscosity, sliding velocity, and ring parameters are known for every point on the h_0 versus μ curves, friction can be calculated for each of those points. Friction is plotted in the lower sections of Figures 6-1, 6-2, and 6-3.

6.4 Discussion

From glancing at the h_0 versus μ plots it can be observed that all of these curves--particularly the ones for h_∞ = 1.0 micron (Figure 6-1, top)--have an upward then downward sloping behavior, like a bell or like an upside down letter "U." The h_0 versus μ curves for the other h_∞ values probably exhibit the same rising and falling behavior, but the range of viscosity covered does not extend high enough to show the falling side of all the curves. The two sides of the curve shall be called the up- and down-branch. Up signifies that h_0 is going up with increasing viscosity; down signifies that h_0 is going down with increasing viscosity. Intuitively, it seems that film thickness should increase with increasing viscosity, but the down-branch contradicts the direct proportionality between film thickness and viscosity. Further investigation reveals that the up- and down-branches can be differentiated by the nature of the calculated pressure distribution under the ring.

The up-branch is characterized by a certain type of pressure distribution which is positive throughout the ring region. The down-branch is characterized by a pressure

distribution which has a negative dip (i.e. the pressure is lower that the exit pressure) on the x_2 (the trailing) side. Figure 6-4 illustrates the two pressure curve shapes that correlate with the two branches of the h_0 versus μ curve. The h_0 versus μ curve for h_∞ = 1.0 micron, σ = 0.023 N/m is repeated from the upper plot of Figure 6-1 for illustrative purposes. The up-branch pressure distribution depicted at the upper left of Figure 6-4 supports the top ring when μ = 0.0065 kg/m-s, and the down-branch pressure distribution depicted at the upper right of Figure 6-4 supports the ring when μ = 0.009 kg/m-s

In principle, both the solutions are satisfactory in that they satisfy the lubrication equation and the boundary conditions for a given σ, h_∞, and ring loading. The down-branch solution, however, could lead to a pressure distribution with a region of significantly negative pressure (i.e. below exit pressure) which will lead to cavitation. Therefore such a solution is not desirable.

The three friction plots behave as expected. Friction decreases with higher film thickness (due to lower shear stress), increases monotonically with viscosity (due to higher shear stress), and decreases with higher surface tension. The exit shear stress boundary condition in the code directly relates the low strain rate surface tension to the shear stress at the exit:

$$\tau_{es} = \frac{\sigma_0}{b}\left(\frac{\partial \sigma}{\partial x}\right)_{ND}\Bigg|_{x_2} \qquad (6.1)$$

where t_{es} is the shear stress at the film detachment point, σ_0 is the low strain rate surface tension, b is the wetted width used as a scaling factor, and $(d\sigma/dx)_{ND}$ is the non-dimensional surface tension gradient at the exit location. Higher surface tension should force the code to find a solution with x_2 closer to the origin where the

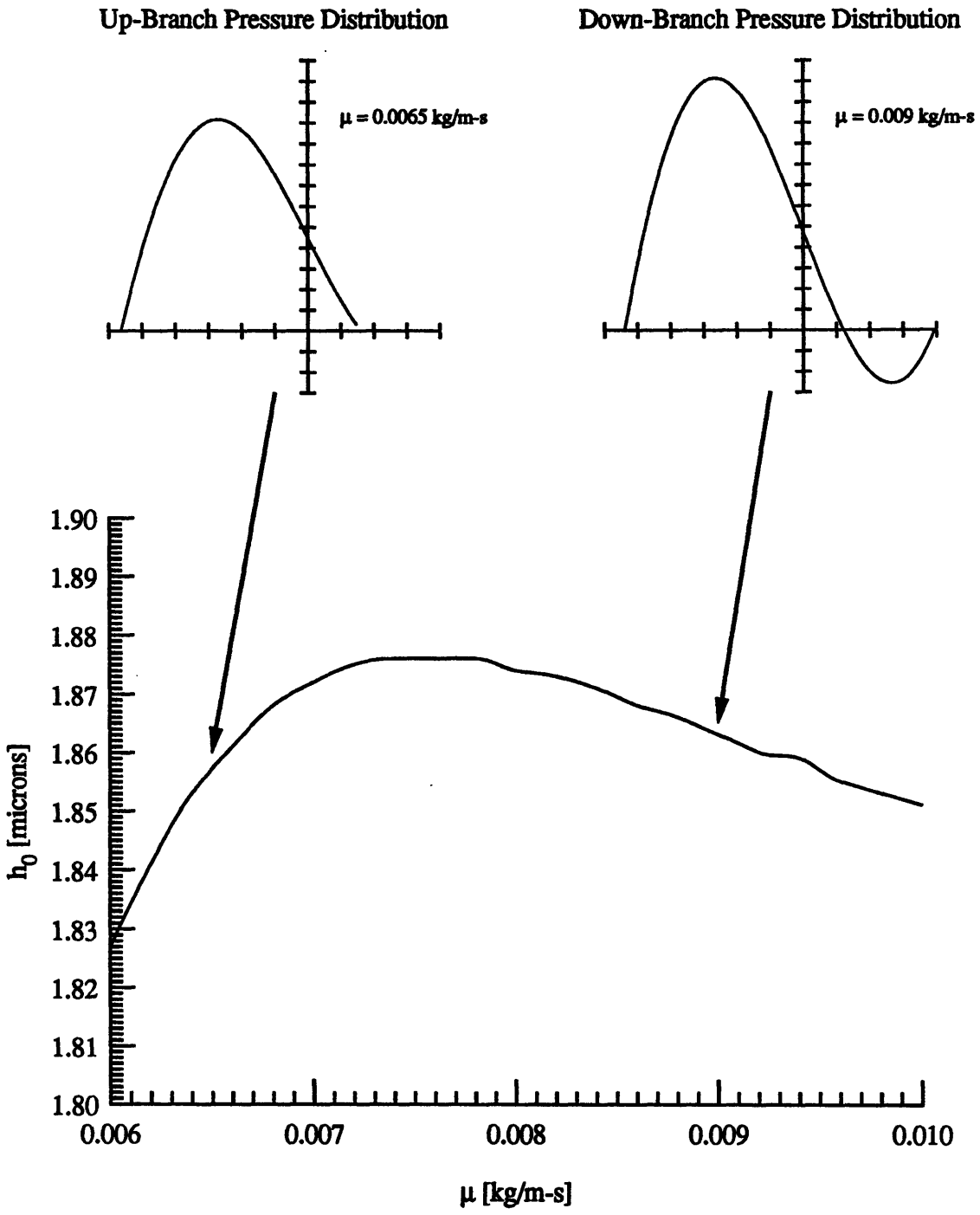

Figure 6-4 Two pressure distribution regimes of the h0 versus viscosity plot (surface tension equals 23 dynes/cm, h(inf) = 1.0 micron).

magnitude of the shear stress is higher (the magnitude of the shear stress is higher in the middle of the ring profile because the ring face is closest to the liner there). When the exit distance is reduced, so is the wetted width. Smaller wetted width is associated with lower friction because the drag shear stress acts over a smaller area of the ring face.

6.5 The Critical Point Between Rising and Falling Branches of the h_0 versus μ Plots

With reference to Figure 6-4, as μ increases at fixed σ, the pressure distribution starts out looking like the up-branch type. Then at some critical value (near 0.0075 kg/m-s for the case in Figure 6-4) the pressure distribution changes character to look like the down-branch type. For a quadratic ring profile, the two conditions which have to be met at the exit are:

$$P^*(x_2^*) = \frac{x_2^*}{2} + \frac{\sin 2x_2^*}{4} - 2\frac{h_\infty}{h_0}\left(\frac{3x_2^*}{8} + \frac{\sin 2x_2^*}{4} + \frac{\sin 4x_2^*}{32}\right) - \left[\frac{x_1^*}{2} + \frac{\sin 2x_1^*}{4} - 2\frac{h_\infty}{h_0}\left(\frac{3x_1^*}{8} + \frac{\sin 2x_1^*}{4} + \frac{\sin 4x_1^*}{32}\right) - P_1^*\right] = P_2^* \quad (6.2)$$

and

$$\tau^*(x_2^*) = 2\cos^2 x_2^* - 6\frac{h_\infty}{h_0}\cos^4 x_2^* = \frac{h_0\sigma_0\bar{\sigma}}{\mu U b} \quad (6.3)$$

Equation (6.2) states the pressure boundary condition at the film detachment location, and equation (6.3) states the exit shear stress boundary condition. The expression for shear stress in (6.3) comes from differentiating the velocity under the parabolic ring profile with respect to y.

The code automatically ensures that these two conditions are met for each solution. While ascending in μ, there is some point at which the x_2^* that satisfies the two conditions is far enough out from the origin to expose the negative dip in the pressure distribution. This critical point can be found numerically by plotting h_0 versus μ and finding the peak in the curve. Figure 6-5 shows the upward trend of $\mu_{critical}$ (the viscosity value at which the slope of the h_0 versus μ curve changes from up to down) with increasing surface tension.

6.6 How Different Pressure Curve Regimes Cause Rising or Falling Behavior

The sub-ring pressure distribution depicted in Figure 6-4 for the up-branch of the h_0 versus μ plot is all positive. For this sort of pressure curve, increasing μ has the effect of increasing the magnitude of the pressures all along the curve. When an all-positive pressure curve is integrated to get a hydrodynamic lift force, higher magnitude pressures result in a greater lift force, given h_0 remains constant. However, it is not h_0 that remains constant but rather ring loading. Since load is fixed, h_0 must increase in order to compensate for increased viscosity. For the all-positive pressure curve, higher viscosity gives rise to higher lift force, but higher h_0 brings the lift force back down so that the supported load stays constant. This explains why h_0 increases with increasing viscosity for the up-branch.

The down-branch is characterized by a different pressure distribution--one that exhibits a negative dip on the x_2 side. Such a pressure distribution is shown in Figure 6-4, upper right. When viscosity is increased at fixed h_0 for this pressure distribution, the hydrodynamic lift force decreases because of the influence of the negative pressure dip. In order to balance the ring load, h_0 must decrease. Therefore, h_0 decreases with increasing viscosity for the down-branch.

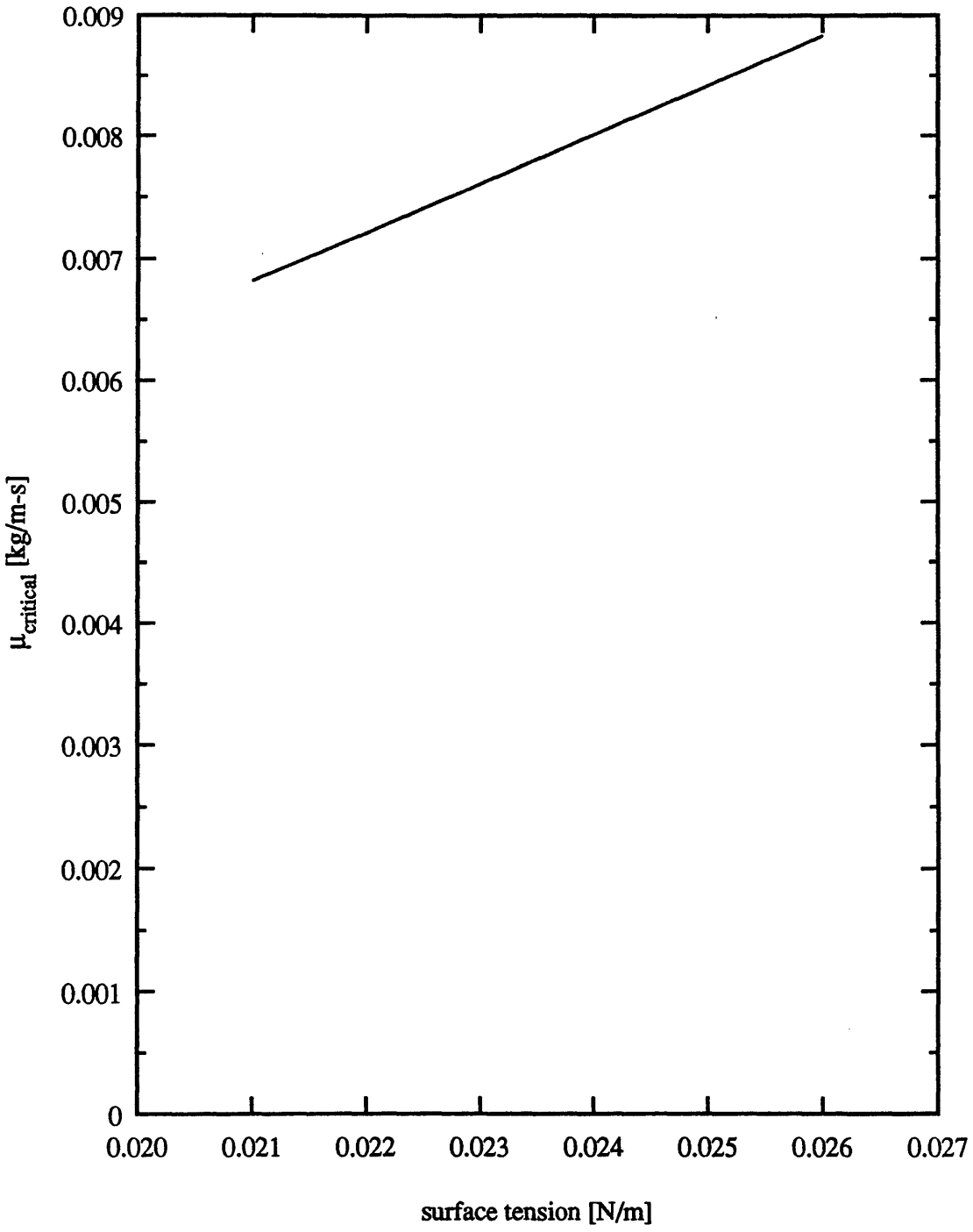

Figure 6-5 Critical viscosity versus surface tension for h(inf) = 1.0 micron.

6.7 Interpreting Maps for Friction Tuning

The h_0 versus μ and friction versus μ plots can be used as maps for lubricant design. For example, say one has a lubricant with a minimum viscosity of 0.0075 kg/m-s specified to maintain adequate film thickness during boundary lubrication at the ends of the piston stroke. Assume that one has an estimate of the cylinder liner oil film thickness at 2.5 microns. Referring to Figure 6-3 for $h_{\infty} = 2.5$ microns, one can expect a friction reduction from 9.3 N/m to 8.1 N/m by changing surface tension from 0.021 N/m to 0.026 N/m. One can also expect a concomitant reduction in mid-stroke film thickness from 4.54 microns to 4.36 microns.

The preceding discussion is based on theoretical results with certain engine conditions and ring parameters as input. The lubricant flow theory is subject to improvement, but these calculations serve to show the sort of lubricant design possible using a top ring oil flow code.

CHAPTER 7: Conclusion

7.1 Major Results

The film behavior in a spark-ignition engine was found to be similar to that in compression-ignition engines. The matrix of experimental lubricants revealed interesting trends in top ring film thickness at mid-stroke, namely that liner oil thickness increases with decreasing viscosity and surface tension. Poor ring fits precluded detailed analysis of wetting information, but improvements in LIF system resolution and the use of a circumferential array of LIF probes should yield better ring fits in the future.

There is a possible explanation for the counter-intuitive trend of rising film thickness with decreasing viscosity. In order for an oil film to get laid down on the upper portion of the cylinder liner, oil must travel from the crankcase and past the ring pack. Numerous flow resistances (oil control ring supply passages, piston/skirt clearance, ring gaps, ring grooves, etc.) along the way make it harder for a high viscosity oil to reach the liner. Assume that the oil film is laid onto the liner during the downstrokes. Oil reaches the OC ring groove either through the OC relief passages or by flowing past the piston skirt. Oil must then get past the OC ring to the third land, squeeze past the second ring (by flowing under the ring face, between the ring and its groove, or through the ring gap) to the second land, and finally squeeze past the top ring to the upper cylinder area. Although a better understanding of the complex flow phenomenon is required in order to fully comprehend the dependence of liner oil film on viscosity, it is significant that a low viscosity oil might supply the liner with a thicker film than a high viscosity oil.

On the theoretical side, the computer model of top ring oil flow was exercised to generate friction predictions for the test oils based on the film thicknesses they exhibited in the engine. Additionally, a parametric study showed the theoretical curves of how sub-ring film thickness and friction vary with viscosity and surface tension.

7.2 Future Work

Efforts are in progress to address the possible bore out-of-round problem. The engine with a circumferential array of LIF probes (see Figure 7-1) will hopefully provide detailed wetting information around the top and second rings. LIF probe locations near the top and bottom of the piston stroke will further the understanding of what happens to the oil film at the ends of the stroke.

The computer model for the oil flow under the top and second rings is under development to extend its capabilities to the ends of the piston stroke. The goal is to fit this code into a complete model for the entire ring pack and piston skirt. Such a model would predict piston friction in the bore as a function of oil properties, ring design, and engine running conditions.

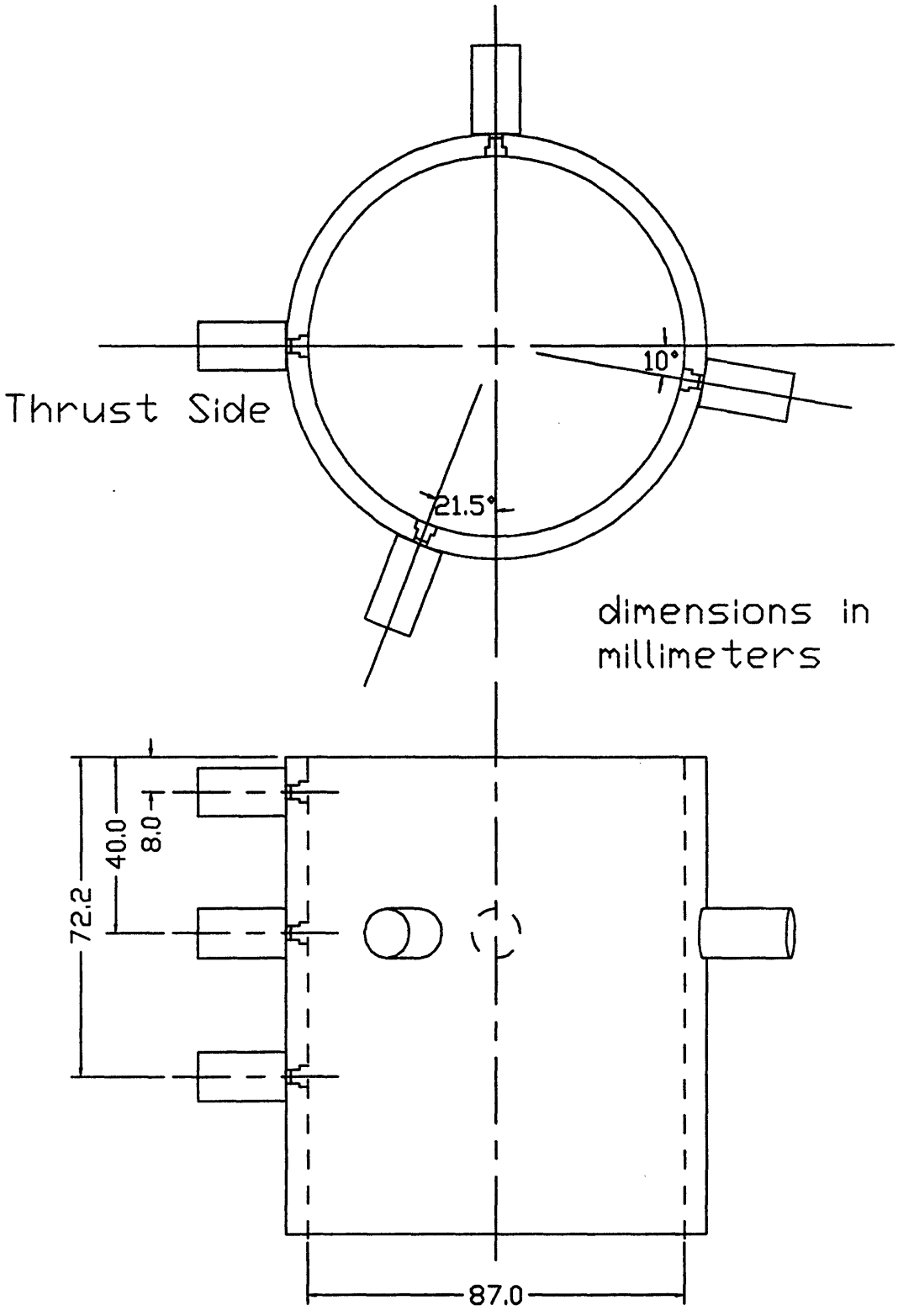

Figure 7-1 LIF probe locations in new Kohler liner.

REFERENCES

1. Heywood, J. B., Internal Combustion Engine Fundamentals, McGraw-Hill Book Company, New York, 1988.

2. Azzola, J. H., "The Role of Surface Tension in the Reduction of Piston Ring Drag," Ph. D. Thesis, Department of Mechanical Engineering, MIT, 1992.

3. Hoult, D. P., Billian, S. A., Lux, J. P., and Wong, V. W., "Calibration of Laser Fluorescence Measurements of Lubricant Film Thickness in Engines," SAE Paper 881587, 1988.

4. Shaw II, B. T., Hoult, D. P., and Wong, V. W., "Development of Engine Lubricant Film Thickness Diagnostics Using Fiber Optics and Laser Fluorescence," SAE Paper 920651, 1992.

5. Lux, J. P., "Lubricant Film Thickness Measurements in a Diesel Engine," S. M. Thesis, Department of Mechanical Engineering, MIT, 1989.

6. Wong, V. W. and Hoult, D. P., "Experimental Survey of Lubricant-Film Characteristics and Oil Consumption in a Small Diesel Engine," SAE Paper 910741, 1991.

7. McElwee, M. R., "Comparison of Single-Grade and Multi-Grade Lubricants in a Production Diesel Engine," S. M. Thesis, Department of Mechanical Engineering, MIT, 1990.

8. Lux, J. P., Hoult, D. P., and Olechowski, M. J., "Lubricant Film Thickness Measurements in a Diesel Engine Piston Ring Zone," Journal of the STLE, Volume 47, 5, 1991, pp. 353-364.

9. Brown, M. A., McCann, H., and Thompson, D. M., "Characterization of the Oil Film Behaviour Between the Liner and Piston of a Heavy-Duty Diesel Engine," SAE Paper 932784, 1993.